



# Diatom-based paleoproductivity and climate change record of the Gulf of Tehuantepec (Eastern Tropical Pacific) during the last ~500 years

The Holocene  
1–16

© The Author(s) 2023





Article reuse guidelines:

sagepub.com/journals-permissions

DOI: 10.1177/09596836231183057

journals.sagepub.com/home/hol



Laura Almaraz-Ruiz,<sup>1</sup> María Luisa Machain-Castillo,<sup>2</sup>   
 Abdelfettah Sifeddine,<sup>3,4</sup> Ana Carolina Ruiz-Fernández,<sup>5</sup>  
 Joan-Albert Sanchez-Cabeza,<sup>5</sup> Alejandro Rodríguez-Ramírez,<sup>2</sup>   
 Perla Guadalupe López-Mendoza,<sup>1</sup> Mercedes Mendez-Millan<sup>3</sup> and  
 Sandrine Caquineau<sup>3</sup>

## Abstract

Changes in marine productivity of the last five centuries in the Gulf of Tehuantepec were investigated using a high-resolution record of diatoms, organic carbon ( $C_{org}$ ), total nitrogen (TN), Ni/Al, and Cu/Al. The laminated sediments were dated by using  $^{210}\text{Pb}$  and  $^{14}\text{C}$ , with a bayesian age model providing a new  $\Delta R = 247 \pm 30$  years for the bulk sediment. The Little Ice Age (LIA) (~1500 to ~1858 CE) was characterized by the predominance of cold-water and high productivity diatoms (*Chaetoceros* spores, *Thalassionema nitzschioides*, *Lioloma pacificum*, *Thalassiosira nanolineata*, and *Rhizosolenia setigera*) and high values of geochemical productivity proxies. A transition period (~1860 to ~1919 CE) toward warmer conditions related to the end of the LIA and the beginning of the Current Warm Period (CWP), was indicated by the appearance of warm-water diatoms (*Neodelphineis pelagica*, *Thalassiosira tenera*, and *Rhizosolenia bergonii*), as well as lower values of  $C_{org}$ , TN, Ni/Al, and Cu/Al. The most recent period of the CWP (~1920 CE to today) was characterized by the increased abundance warm-water taxa (*N. pelagica*, *Cymatodiscus planetophorus*, *T. tenera*, *Plagiogramma minus*, *Nitzschia interruptestriata*, and *R. bergonii*), and by the prevalence of low values of  $C_{org}$ , TN, Ni/Al, and Cu/Al. These changes in productivity during the LIA and CWP were likely driven by changes in solar irradiance and the migration of the Intertropical Convergence Zone. This study highlights the spatial extent of the LIA in the Eastern Tropical North Pacific and contributes to the knowledge of the productivity response to climate in tropical regions.

## Keywords

current warm period, diatoms, Gulf of Tehuantepec, Little Ice Age, paleoproductivity, upwelling

Received 12 October 2022; revised manuscript accepted 18 April 2023

## Introduction

The climate of the Eastern Tropical North Pacific (ETNP) is primarily modulated by changes in the strength of the trade winds and the latitudinal shifts of the Intertropical Convergence Zone (ITCZ) (Lavín et al., 2006). Also, variations at diverse scales (centennial, decadal and interannual) have impacted the ETNP climate in the last half millenium . A prolonged cold period called the Little Ice Age (LIA ~1250 to ~1850 CE, e.g. Crowley et al. (2008), Miller et al. (2012), ~1400 to ~1700 CE, e.g. Mann et al., 2009) has been related to the lowest solar irradiance in the past millenium (Spörer, Maunder and Dalton solar minima, Bard et al., 2000; Lean, 2018), and increased volcanic activity (Crowley et al., 2008). Although the LIA has been widely studied, its timing and impact on a global scale are still being discussed, mainly in tropical regions (Juárez et al., 2014) and in the ETNP (Barron and Bukry, 2007; Choumiline et al., 2019; Goni et al., 2006; Juárez et al., 2014; Staines-Urías et al., 2009). In paleolimnological studies in central and southern Mexico, the LIA has been associated with temperature decrease of ~2.0°C and mountain glacier advance (Lozano-García Mdel et al., 2007; Vázquez-Selem, 2011). A change to warmer

condition is documented worldwide since ~1850 (IPCC, 2014) identified as the Current Warm Period (CWP) (e.g. Griffiths et al., 2016; Salvattecí et al., 2014).

<sup>1</sup>Posgrado en Ciencias del Mar y Limnología, Universidad Nacional Autónoma de México, México

<sup>2</sup>Unidad Académica de Procesos Oceánicos y Costeros, Instituto de Ciencias del Mar y Limnología, Universidad Nacional Autónoma de México, México

<sup>3</sup>IRD, CNRS, SU, MNHN, IPSL, LOCEAN: Laboratoire d'Océanographie et du Climat: Expérimentations et Approches Numériques, France

<sup>4</sup>ERC2- Université Quisqueya, Haïti

<sup>5</sup>Unidad Académica Mazatlán, Instituto de Ciencias del Mar y Limnología, Universidad Nacional Autónoma de México, México

## Corresponding author:

María Luisa Machain-Castillo, Unidad Académica de Procesos Oceánicos y Costeros, Instituto de Ciencias del Mar y Limnología, Universidad Nacional Autónoma de México, Circuito Exterior s/n, Ciudad Universitaria, Ciudad de Mexico 04510, México.

Email: machain@cmarl.unam.mx

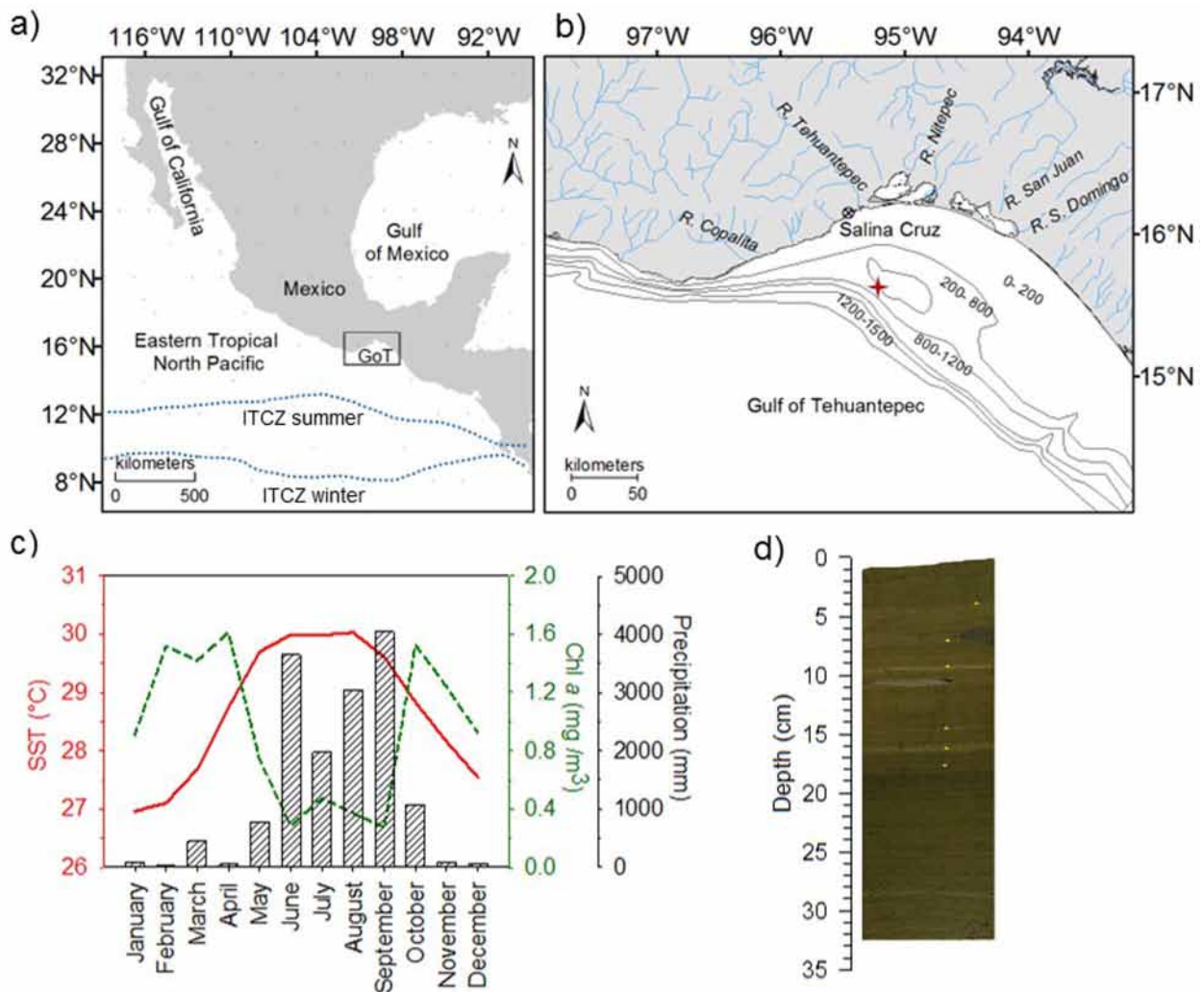


**Figure 1.** (a) Gulf of Tehuantepec (GoT) location in the Eastern Tropical North Pacific and mean position of the ITCZ in summer and winter (Amador et al., 2006). (b) sampling site of core Tehua XII E03 (red star) and main rivers in the Tehuantepec coast. (c) Monthly average of Sea Surface Temperature (SST), Chlorophyll *a* (Chl *a*), and Precipitation in the study area (data taken from IRI, 2015). (d) Photograph of core Tehua XII E03b, the yellow asterisks indicate the key laminae used to correlate subcores.

The Gulf of Tehuantepec (GoT) is in the ETNP (Figure 1). Water masses in the GoT are: Equatorial Surface Water (ESW, up to 29°C and salinity >34), Subtropical Subsurface Water (SSW, <25°C and salinity >35), North Pacific Intermediate Water (NPIW, 4°C–9°C and salinity <34.5), and North Deep Pacific Water (NDPW, 1.2°C–2°C, <34.5) (Fiedler and Talley, 2006; Machain–Castillo et al., 2008); and their vertical distribution is influenced by the atmospheric circulation regime.

During winter and early spring seasons, the ITCZ is located at its southernmost position, and easterly trade winds across southern Mexico and Central America are stronger than the rest of the year (Amador et al., 2006). These conditions allow the high-pressure systems south-eastward migration associated with cold-air outbreaks coming from the northwestern United States. The outbreaks generate airflows channeled through the low elevation gap of the Sierra Madre del Sur and reach the GoT as intense northerly winds (Amador et al., 2006), locally named Tehuanos (Trasviña et al., 1995). Tehuanos are perpendicular to the coast and cause mixing and stress curling of the surface water column on the wind axis (Trasviña et al., 1995). These winds can break up the stratification or raise the thermocline near the surface (Kessler, 2006) to even less than ~30m depth (Lluch-Cota et al., 1997), and cold (~20°C), nutrient-rich subsurface waters fertilize the euphotic zone resulting in high primary productivity, including diatom blooms, as revealed by high chlorophyll-*a* concentrations (Figure

1). At this time, the ESW occupied the upper 35–40 to 70m, the SSW is found until 430–470m, the NPIW to 900–1200m, and the NDPW below this depth (Machain–Castillo et al., 2008).

In contrast, during the summer and autumn seasons, the ITCZ is at its northernmost position, rainfall dominates in the ETNP due to the associated convective belt of the ITCZ, and trade winds are weaker than during the winter-spring period (Amador et al., 2006). Surface water circulation is dominated by tropical waters from the equatorial region flowing north through the Costa Rica Coastal Current (Kessler, 2006). The ESW is found between 55 and 70m, SSW until 450m, and the NPIW and NDPW depth limits are similar to winter (Fiedler and Talley, 2006; Machain–Castillo et al., 2008). Tehuanos are relatively sporadic and weak (Romero-Centeno et al., 2007), and the thermocline is deeper at ~70m (Lluch-Cota et al., 1997). Hence upwelling and productivity decrease (Meave del Castillo and Hernández-Becerril, 1998), and the highest sea surface temperatures (SST) ~30.0°C are found (Figure 1).

Diatoms are unicellular algae and one of the main components of phytoplankton in the GoT, together with cyanophytes, dinoflagellates, and coccolithophorids (Meave del Castillo and Hernández-Becerril, 1998). One must consider that preserved diatoms silicate frustules on the seafloor may be a mixed assemblage (freshwater, marine, benthic, and planktonic). Furthermore, most of the information is lost during settling to the seafloor

by dissolution, grazing, transport, reworking, and bioturbation (Crosta and Koc, 2007). However, upwelling regions with high productivity usually reflect the overlaying hydrographic conditions of the surface waters (Treppe et al., 1996), and have been used to reconstruct ocean environmental conditions during climate episodes such as the LIA and the Medieval Warm Period (MWP ~900 to ~1200 CE, e.g. Barron and Bukry, 2007; Barron et al., 2003). In addition, geochemical proxies such as organic carbon ( $C_{org}$ ) and total nitrogen (TN) in sediments have been widely used to infer exported production to the seabed (Sifeddine et al., 2008; Choumiline et al., 2019; Salvatelli et al., 2014). The C:N ratio and  $\delta^{13}C$  have been used to track the origin of sedimentary  $C_{org}$ , since marine phytoplankton and land vegetation carry a distinct C:N and  $\delta^{13}C$  signal (Lamb et al., 2006). Ni and Cu concentrations are also used as productivity tracers since they are used as a micronutrient for the phytoplankton (Smrzka et al., 2019; Tribovillard et al., 2006). Although, these elements can be affected by terrestrial input (Calvert and Pedersen, 2007; Smrzka et al., 2019), the normalization with a terrigenous element (such as Al or Ti) removes the terrestrial signal. Contamination by human impact is another factor that can alter trace element concentrations in sedimentary records (e.g. Ruiz-Fernández et al., 2004). In the GoT coastal zone, previous studies have reported increments in trace metal associated with the development of anthropogenic land-based activities, mainly oil production, urban wastes, and agricultural residues (Pica-Granados et al., 1994; Ruiz-Fernández et al., 2004). Ruiz-Fernández et al. (2004) reported that Cu background level in sediments (before 1860) was 138.9 mg/kg, and a moderate anthropic influence on Cu (from 150 to 480 mg/kg) since the 1980s off Salina Cruz at ~240 m water depth. Concerning Ni, Pica-Granados et al. (1994) reported current high Ni concentrations in water (from 49.8 to 81.7 mg/l) collected near the “Antonio Dovalí Jaime” oil refinery (~5 km from Salina Cruz Port, Figure 1) at <5 m water depth.

Redox processes can also affect the Ni and Cu signals deposited in hypoxic environments (Calvert and Pedersen, 2007; Smrzka et al., 2019). However, when Ni and Cu profiles have similar trends to other productivity proxies, such as  $C_{org}$  and biogenic silica, they can be considered as reliable productivity tracers.

In the GoT, most of the studies on phytoplankton have been focused on taxa distribution, species richness (Torres-Ariño et al., 2019 and references therein), and seasonal variability (e.g. Meave del Castillo and Hernández-Becerril, 1998; Moreno-Ruiz et al., 2011). This study provides the first high-resolution reconstruction of paleoproductivity based on diatoms,  $C_{org}$ , TN, Ni/Al, and Cu/Al of the last five centuries in a sequence of laminated sediments from the GoT and its relationship to ocean-climate variability. The study site is in a more tropical latitude. Nevertheless, we expect that the climate variability of the last centuries seen in more northern regions (e.g. Barron and Bukry, 2007; Choumiline et al., 2019; Goni et al., 2006; Juárez et al., 2014; Staines-Urías et al., 2009) can also be registered in the GoT sediments. Tropical climates are naturally sensitive to climate variations (e.g. Li et al., 2020; Yamaguchi and Suga, 2019), as small SST increases further strengthen upper water column stratification (Amador et al., 2006; Fiedler and Talley, 2006), affecting productivity due to lower nutrient availability (Li et al., 2020; Yamaguchi and Suga, 2019). Therefore, this study helps to understand the effects of warming on tropical regions and their implications for future climate and ocean dynamics.

## Material and methods

### Sediment core

The present study is based on a Reineck box core, retrieved in March 2014 from the GoT (Tehua XII E03, 15.6442° N and

95.3071° W) at 743 m water depth, aboard the R/V “El Puma” from the National Autonomous University of Mexico (UNAM) (Figure 1). Two subcores were obtained; subcore Tehua XII E03a (34.5 cm long, 6.5 cm diameter) was used for  $^{210}Pb$  dating, Ni, and Cu analysis, and subcore Tehua XII E03b (32.5 cm long and 14 × 14 cm wide and high; Figure 1) was used for diatom, and the rest of geochemical analyses ( $C_{org}$ , TN, and  $\delta^{13}C$ ), and radiocarbon ( $^{14}C$ ) dating.

### Age dating

The radiochronology of the upper core segment (0–20 cm) of the subcore Tehua XII E03a was estimated through the  $^{210}Pb$  age dating method at 1 cm resolution (Table S1).  $^{210}Pb$  activities were determined at the laboratory of Isotopic Geochemistry and Geochronology at UNAM (Mexico) through high-resolution gamma ray spectrometry (HPGe well detector, Ortec-Ametek) as described by Díaz-Asencio et al. (2020). For validation,  $^{239,240}Pu$  was determined in selected sediment samples by alpha spectrometry (Ortec-Ametek Alpha Spectrometry system) (Ruiz-Fernández et al., 2014). Data quality was assessed through the analysis of the reference material IAEA-300 (Radionuclides in Baltic Sea sediment) and the results were within the reported range of recommended values.

Radiocarbon ages were determined by accelerator mass spectrometry (AMS), at the National Platform LMC14, France, on five bulk sediment samples (4.0–4.5, 8.0–8.5, 20.0–20.5, 25.0–25.5, and 29.0–29.5 cm depth) of the subcore Tehua XII E03b (Table S2). We used the bulk sediment because of the poor preservation (Arellano-Torres et al., 2013) and recalcification of planktonic foraminiferal shells (Gibson et al., 2016). Previous studies in the GoT using AMS  $^{14}C$  age dating on bulk sediment (Table 1) have shown that this method is reliable in the area (e.g. Arellano-Torres et al., 2013; Blanchet et al., 2012; García-Gallardo et al., 2021; Pichevin et al., 2010). To produce an integrated  $^{210}Pb$ - $^{14}C$  age model, both subcores were stratigraphically correlated by identifying common key laminae (light laminae visually identified in both subcores; Figure 1, Table S1) and  $^{210}Pb$ -derived dates for subcore Tehua XII E03a were transferred to subcore Tehua XII E03b (Table S1).

### Geochemical procedures

Twenty-four dry sediment samples (~0.5 cm each) ground in a porcelain mortar, were used for geochemical analyses at the ALY-SES platform (IRD/SU, Bondy France). The content of  $C_{org}$  and TN and the stable carbon isotopic ratio  $^{13}C/^{12}C$  of the organic matter were determined on a Flash HT 2000 elemental analyzer, coupled to an isotopic ratio mass spectrometer Delta Vplus via a combustion-ConFlow IV interface from Thermo Fischer Scientific. The samples for  $C_{org}$  and  $\delta^{13}C$  analysis were treated with HCl 10% for removal of the carbonate fraction. Bulk sediment was used for TN analysis. The stable carbon isotopic ratio  $^{13}C/^{12}C$  of OM is reported in the conventional  $\delta$ -notation with respect to the PDB (Pee Dee Belemnite) carbonate standard defined with the equation  $\delta^{13}C = \frac{^{13}C / ^{12}C_{sample} - ^{13}C / ^{12}C_{standard}}{^{13}C / ^{12}C_{standard}} * 1000$ .

The analytical precision was determined by replicates of the certified reference materials and was always below 0.12% for  $C_{org}$  and TN, and lower than  $\pm 0.2\text{‰}$  for  $\delta^{13}C$ . The  $\delta^{13}C$  values are expressed in ‰ against the international standard PDB.

To evaluate the productivity changes along the core, Ni and Cu concentrations were used as productivity proxies (Smrzka et al., 2019; Tribovillard et al., 2006). As the Ni and Cu concentration in the sediments can be affected by terrestrial input, we normalized them with Al concentrations (Calvert and Pedersen, 2007). Ni,

**Table 1.** Ages, reservoir age applied and sedimentation rate from nearby cores to Tehua XII E03.

Core	Sampling method	Material	Interval (cm)	Calibrated <sup>14</sup> C Age ( <sup>14</sup> C yr BP)	Calibrated <sup>14</sup> C Age (yr CE)	Reservoir age (years)	Reservoir age applied	Rate sedimentation (cm/yr)	Authors
ME0005A0-3TC	Associated trigger corer	<i>Bolivina</i> spp.	0–4.0	1760	1307	400		0.04–0.07	Thunell and Kepple (2004)
ME0005A-3JC	Jumbo piston corer	<i>Bolivina-Uvigerina</i> spp.	2.0–3.0 16.0–18.0	2530 2870	244 164	400		0.04–0.07	Thunell and Kepple (2004)
ME0005A-3JC	Jumbo piston corer	<i>Bolivina-Uvigerina</i> spp.	2.0–3.0 16.0–18.0	2530 2870	260 710	0		0.06	Hendy and Pedersen (2006)
ME0005A-3JC	Jumbo piston corer	<i>Bolivina plicata</i>	2.5 17	2530 2870	47 475	450 ± 50		0.06	Arellano-Torres et al. (2013)
MD02-2520	Calypso piston corer	Organic carbon	1	–	1435	450 ± 50		0.1	Pichevin et al. (2010), Blanchet et al. (2012), Arellano-Torres et al. (2013)
MD02-2523	Calypso piston corer	<i>Bolivina plicata</i>	6	1800	755	450 ± 50		0.02	Arellano-Torres et al. (2013)
MD02-2521C <sup>2</sup>	Square Calypso Corer	Bulk marine sediment	0.1–0.6 9.0–10.0	1012 1152	1466 1392	458 ± 51		0.08–0.12	García-Gallardo et al. (2021)
Tehua XII E03	Reineck box corer	Bulk marine sediment	4.0–4.5 8.0–8.5 20.0–20.5	695 850 965	1978 1944 1798	>456 ± 51 ΔR = 247 ± 30 years		0.08–0.14	This study

Cu, and Al concentrations were determined on 35 samples (~1 cm each) by X-ray fluorescence spectrometry (XRF, Spectrolab Xepos-3). Analytical precision was assessed through the replicate analysis ( $n=3$ ) of a single sediment sample, and the coefficients of variation were  $<0.6\%$  for Ni and Cu, and  $<0.01\%$  for Al). The accuracy of the measurements was evaluated through the analysis of the reference material IAEA-158 with results obtained within the reported certified values.

### Diatom processing

Ninety-two sediment samples (~0.4 cm average thickness and ~6 years temporal resolution average; Table S3) were obtained for diatom analysis. Samples were processed at the Micropaleontology Laboratory of the Marine Sciences and Limnology Institute, UNAM. Laminae were visually recognized and separated using an x-ray digitalized acetate template. The dry weight of each sediment lamina was registered for abundance calculations. Sediment samples (~0.2 to ~0.5 g dry weight) were added with HCl 10% to eliminate carbonates and digested at ~80°C with H<sub>2</sub>O<sub>2</sub> 30% and HNO<sub>3</sub> 70% to remove organic matter. Acids and salts were removed through several washes with distilled water, settled for at least 24 h, and the liquid was discarded. The samples were diluted to a standard volume (30 mL).

For diatom slides, samples were homogenized and 200 µL aliquots were taken. In most samples, dilution was needed owing to the large number of particles, these volumes were considered for the calculation of total abundance. Aliquots were placed on coverslips (18 mm diameter) and dried at room temperature. Slides were mounted in Naphrax resin (refraction index = 1.74). All diatoms were identified at the genera or species taxonomic level using Cupp (1943), Round et al. (1990), Moreno et al. (1996), Hasle and Syvertsen (1997), Hernández-Becerril et al. (2021), and specialized literatures. The samples were counted by transects (Schrader and Gersonde, 1978), at least 500 valves per sample were identified under a light microscope (Nikon eclipse Ni) at 1000x magnification with Nomarski interference contrast. The precision of the diatom analysis was evaluated through the replicate analysis ( $n=8$ ) of diatom slides; the relative standard deviation was  $<8\%$ . The species composition is reported as relative abundance (%).

### Data analysis

In order to quantitatively define assemblages' zone (periods) in the studied core, a CONISS (CONstrained Incremental Sums of Squares; Grimm, 1987) analysis was applied to a simplified diatom species matrix (taxa with total abundances  $>0.8\%$ ; Table S3) together with geochemical data ( $C_{org}$ , TN,  $\delta^{13}C$ , C:N, Ni/Al, and Cu/Al). A squared Euclidian matrix approach was used to quantify the dissimilarity between samples, and the number of statistically significant zones was established with a broken stick model (Bennett, 1996). These procedures were performed with the R packages "rioja" (Juggins, 2020) and "vegan" (Oksanen et al., 2020).

## Results

### Age-depth model

The <sup>210</sup>Pb chronology was established a) with the Constant Flux model (Sanchez-Cabeza and Ruiz-Fernández, 2012), with uncertainties estimated through a Monte Carlo method with 10<sup>6</sup> simulations (Sanchez-Cabeza et al., 2014), and b) with a bayesian method (Aquino-López et al., 2018) by using the R package rplum (Blaauw et al., 2021), which has been successfully used in contrasting aquatic environments, including marine sediment cores (Aquino-López et al., 2020). Both chronologies were almost

identical and were successfully validated with the <sup>239,240</sup>Pu onset, which is a robust age-dating marker in regions far from nuclear testing grounds (Sanchez-Cabeza et al., 2021) (Figure 2).

Following common practice, the radiocarbon ages were calibrated with the Marine20 curve (Heaton et al., 2020) and corrected for a regional marine reservoir age ( $\Delta R$ ) of  $456 \pm 51$  years (Berger et al., 1966), but ages of sections 4.0–4.5 and 8.0–8.5 were significantly older than the <sup>210</sup>Pb-derived ones (Table S1-S2). These discrepancies have been attributed to regional differences in the marine reservoir age (e.g. Hendy and Pedersen, 2006; Thunell and Kepple, 2004), which can be large in upwelling areas (Goodfriend and Flessa, 1997; Gutiérrez et al., 2009).

To estimate the local  $\Delta R$ , we followed the method described by Reimer and Reimer (2017), which has been successfully used with <sup>210</sup>Pb in the Baja California continental margin, also affected by upwelling (Treinen-Crespo et al., 2021). To calculate uncertainties, we used a Monte Carlo approach with the R language (R Core Team, 2021). The <sup>210</sup>Pb-derived ages were expressed as BP (before present; age BP = 1950 – calendar age) and produced 10<sup>6</sup> simulations of the <sup>210</sup>Pb age BP (*pb210.bp*) and the sample radiocarbon age (*c14*) following normal distributions. Simulated <sup>210</sup>Pb BP ages younger than 1950 were discarded as they could not be calibrated with the MARINE20 curve. Each *pb210.bp* simulation was reverse-calibrated with the MARINE20 curve (*pb210.c14*) by using the *calBP.14C* function of the IntCal package (Blaauw, 2022). Then, the  $\Delta R$  simulations were determined as the difference between the sample radiocarbon age simulations (*c14*) and the <sup>210</sup>Pb reverse-calibrated age simulations (*pb210.c14*) as  $\Delta R = c14 - pb210.c14$ . Finally,  $\Delta R$  and its uncertainty were determined as the mean and standard deviation of all simulations, respectively ( $\Delta R = 247 \pm 30$  years, 1 sigma).

The integrated <sup>210</sup>Pb-<sup>14</sup>C age-model was produced by a bayesian approach (Blaauw and Christen, 2011) with the rbacon R package (Blaauw et al., 2022). We used all <sup>210</sup>Pb-derived ages and the three radiocarbon <sup>14</sup>C ages beyond the validated <sup>210</sup>Pb chronology (sections below 20.0 cm), with the MARINE20 curve and the calculated  $\Delta R$ . The integrated age-model showed a satisfactory agreement between <sup>210</sup>Pb and <sup>14</sup>C ages, and a common and smooth trend (Figure 3).

The integrated <sup>210</sup>Pb and <sup>14</sup>C age model indicated that the base of the core reached ~1500 CE (Table S4; Figure 3). The average sediment accumulation rate from ~1907 to ~2014 CE was  $0.14 \pm 0.07$  cm/year; whereas for the older sediment, the sedimentation rate was of  $0.08 \pm 0.06$  cm/year (Tables S1 to S2).

### Geochemistry

The  $C_{org}$  (%) and TN (%) trends were similar along the core, with values ranging from 4.94 to 7.33% (average  $C_{org} = 6.35\%$ ) and 0.52 to 0.87% (average TN = 0.68%), respectively. Both elements displayed the highest values between ~1717 and ~1820 CE. The  $\delta^{13}C$  varied from -21.24 to -18.22‰ (average  $\delta^{13}C = -19.40\%$ ) (Figure 4; Table S3). The Ni/Al ranged from 0.01 to 0.11 (average = 0.50), Cu/Al from 3.55 to 8.25 (average = 5.58) (Table S3). From ~1500 to ~1847 CE, Ni/Al and Cu/Al showed the highest concentrations (Figure 4).

### Diatoms

A total of 103 taxa belonging to 54 genera were determined; marine taxa were predominant and benthic and freshwater taxa represented only  $< \sim 9\%$  of all studied sample. Specimens in the sediment core Tehua XII E03 were common to adjacent tropical Pacific regions and other upwelling areas. Seventeen taxa with a total relative abundance  $>0.8\%$  made up 85.8% (Figure 4; Plate 1; Table S3). *Thalassionema nitzschoides* (20.9%) and *Chaetoceros* spores (mainly *C. affinis*, *C. costatus*, *C. curvisetus*, and *C.*

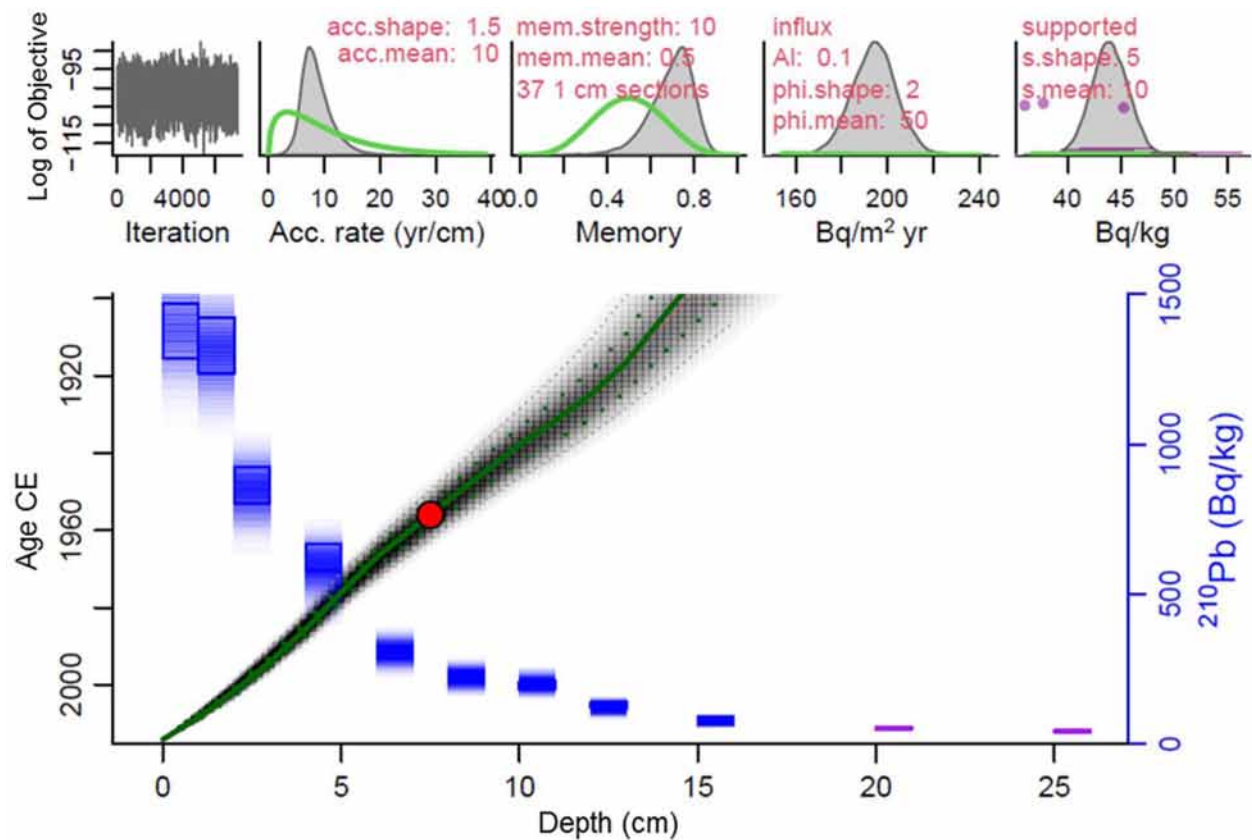


**Figure 2.**  $^{210}\text{Pb}$ -derived age model for the core Tehua XII E03 using the Constant flux (green line) and Plum models (red line). The blue squares represent the  $^{210}\text{Pb}$  activities ( $\pm 2\sigma$ ; right axis). The red point represents the  $^{239,240}\text{Pu}$  onset (red point) in 1954 CE (Common Era), used to validate the age model.

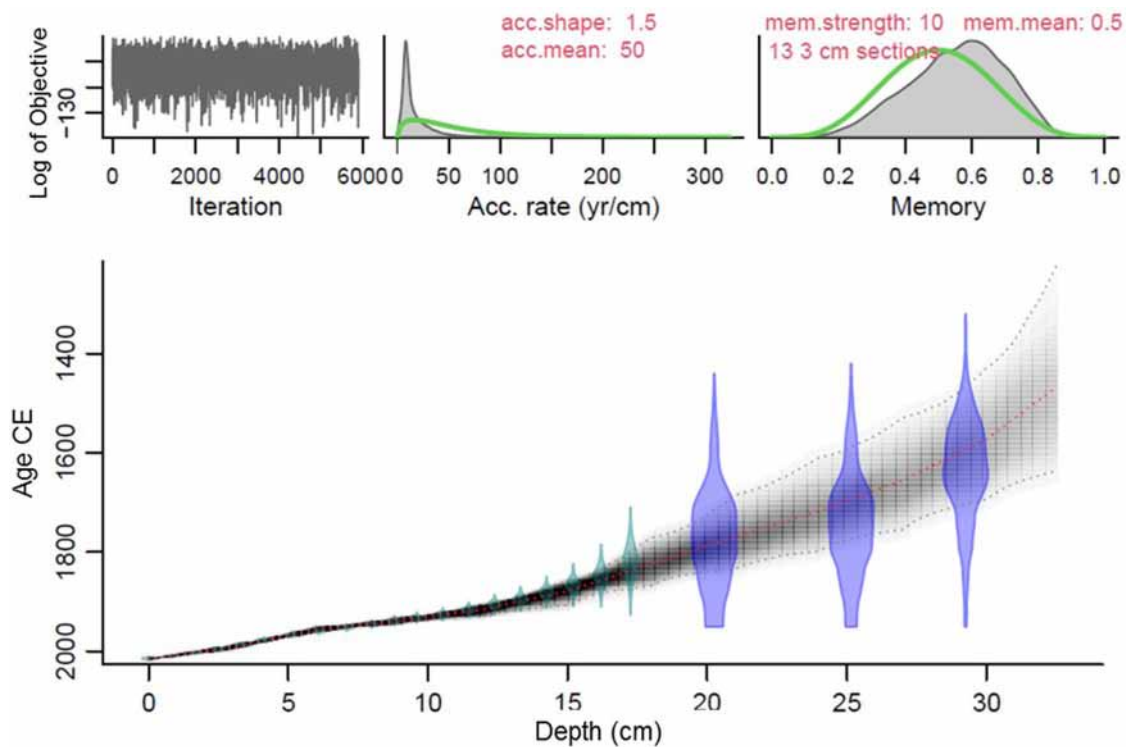


**Figure 3.** Integrated Bayesian age model of the core Tehua XII E03 using MARINE20 curve and the calculated  $\Delta R = 247 \pm 30$  years.  $^{210}\text{Pb}$  dates in cyan color and  $^{14}\text{C}$  dates in blue. CE=Common Era.

*radicans*) (18.5%) were the dominant taxa, reaching up to 57% of total assemblages in the samples; followed by *Neodelphineis pelagica* (8.5%), *Thalassionema bacillare* (6.6%), *Lioloma*

*pacificum* (5.8%), *Thalassionema nitzschioides* var. *parvum* (5.0%), *Fragillariopsis doliolus* (4.4%), *Cyclotella litoralis* (3.1%), *Thalassiosira oestrupii* (3.0%), *Thalassiosira*

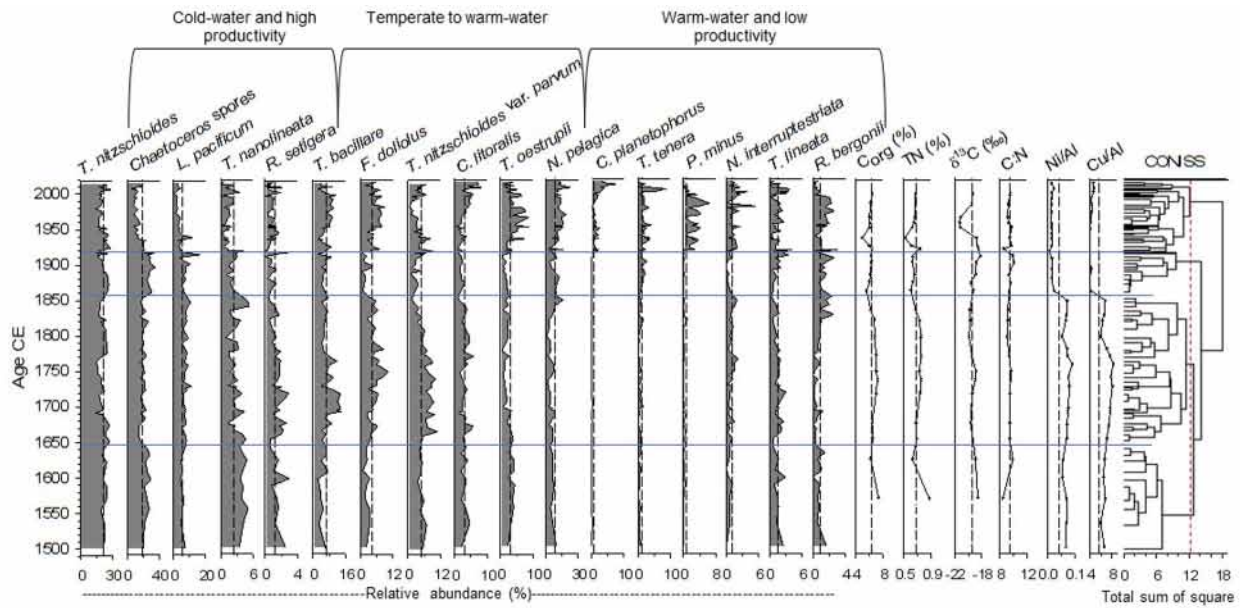


**Figure 4.** Relative abundance (%) and ecological group for the most common diatoms (>0.8%),  $C_{org}$  (%), TN (%),  $\delta^{13}C$  (‰), C:N, Ni/Al, Cu/Al, and CONISS dendrogram of the Tehua XII E03. Vertical dashed lines indicate the average values of each set. Horizontal (blue) lines indicate the four zones defined by CONISS analysis (at the 12.1 of total sum of squares indicated in red dotted line).

*nanolineata* (2.4%), *Rhizosolenia setigera* (1.5%), *Thalassiosira lineata* (1.4%), *Thalassiosira tenera* (1.4%), *Nitzschia interruptestriata* (1.1%), *Rhizosolenia bergonii* (0.9%), *Plagiogramma minus* (0.8%), and *Cymatodiscus planetophorus* (0.8%).

#### Ecological affinity of the main diatom taxa in the Gulf of Tehuantepec

*Thalassionema nitzschioides* is widely distributed from tropical to temperate waters (Hasle and Syvertsen, 1997) and usually appears throughout the year (Meave del Castillo, 2002; Meave del Castillo and Hernández-Becerril, 1998; Romero et al., 2009a; Sancetta, 1995); however, its largest abundance in subtropical to tropical regions occurs during the most productive season (e.g. Almaraz-Ruiz, 2017; Barron et al., 2010; Romero et al., 2011; Sancetta, 1995; Schrader et al., 1993; Treppke et al., 1996). Similarly, the *Chaetoceros* genus is usually predominant in regions with high nutrient availability (Hasle and Syvertsen, 1997; Lange et al., 1997; Meave del Castillo, 2002; Meave del Castillo and Hernández-Becerril, 1998; Rines and Hargraves, 1988; Romero et al., 2001, 2009a; Treppke et al., 1996), where it is commonly represented by resting spores in the sediment (e.g. Ren et al., 2014; Romero et al., 2009a; Sancetta, 1995). Unpublished data from sediment traps (~500 m depth) in the sediment core location during an ENSO-neutral year (February to July 2006) indicate that *T. nitzschioides* was more abundant during the most productive season, together with the *Chaetoceros* genus and *L. pacificum*, where *Chaetoceros* was represented mainly by coastal species in their vegetative forms (*C. affinis*, *C. compressus*, *C. costatus*, *C. curvisetus*, *C. decipiens*, *C. diversus*, *C. laciniosus*, *C. lorenzianus*, and *C. radicans*). Resting spores were only found for *C. affinis*, *C. compressus*, *C. costatus*, *C. curvisetus*, and *C. radicans* (Plate 1). In the sediments of core Tehua XII E03, no vegetative forms were found, only resting spores. We identified mainly four resting spore forms (*C. affinis*, *C. costatus*, *C. curvisetus*, and *C. radicans*; Plate 2, 7–10) that correspond to the most abundant *Chaetoceros* taxa found in the sediment traps during the upwelling season. Also, in the core sediments, the highest abundances of *Chaetoceros* spores occurred with *T. nitzschioides* and *L. pacificum*, as in the sediment traps during upwelling events. Therefore, we considered that the association of

*Chaetoceros* spores, *T. nitzschioides* and *L. pacificum* recovered from the GoT sediments reflects the upwelling season conditions.

*Rhizosolenia setigera* is sometimes found together with *Chaetoceros* in the California Current System, reflecting high productivity (Lange et al., 1997; Sancetta, 1995; Sautter and Sancetta, 1992). *Thalassiosira nanolineata* is recorded in Panama Basin as a coastal taxon; however, the species also showed a high factor score in the high productivity group (Romero et al., 2011, Table 1). Since in this study *T. nanolineata* exhibited its highest abundance together with *T. nitzschioides*, *Chaetoceros* spores, *L. pacificum*, and *R. setigera*, it was considered part of the assemblage of cold-waters and high-productivity taxa.

In the California Current System and the Eastern Equatorial Pacific, during warm and low productivity conditions, diatom assemblages are composed of one or more of the following species: *F. doliolus*, *T. oestrupii*, *N. interruptestriata* (Barron et al., 2010, 2013; Lange et al., 1987, 1990; Romero et al., 2011; Sancetta, 1992, 1995; Sautter and Sancetta, 1992; Schrader et al., 1993), *T. bacillare* (Baumgartner et al., 1985), *T. nitzschioides* var. *parvum* (Romero et al., 2011), *T. lineata*, *R. bergonii* (Baumgartner et al., 1985; Kemp et al., 2000; Lange et al., 1987), *C. litoralis* (Barron and Bukry, 2007; Barron et al., 2004, 2005; Sancetta, 1995), *C. planetophorus* (Estrada Gutiérrez et al., 2022), *N. pelagica* (Almaraz-Ruiz, 2017), and other taxa in minor amounts. In particular, *R. bergonii* is a deep-dwelling taxon (up to ~130 m, Kemp et al., 2000) that indicates strong stratification in the water column in tropical to subtropical regions (Baumgartner et al., 1985; Kemp et al., 2000; Lange et al., 1987, 1994; Romero et al., 2011). For example, in the Santa Barbara Basin, *R. bergonii* (and other warm-water diatoms) showed high abundances during the 1983 El Niño (Lange et al., 1987). This trend also was observed in the Guaymas Basin during the 1957–1959, 1965, 1968–1969, and 1972 El Niño events (Baumgartner et al., 1985). El Niño on the Eastern North Pacific coast are characterized by a strong upper water column stratification and a deeper thermocline, which limit nutrients availability, and consequently low productivity (Pennington et al., 2006), where *R. bergonii* is one of the common species. However, some of these species have also been observed in temperate water, such as *F. doliolus* (Almaraz-Ruiz, 2017; Lange et al., 1994; Sancetta, 1995; Treppke et al.,

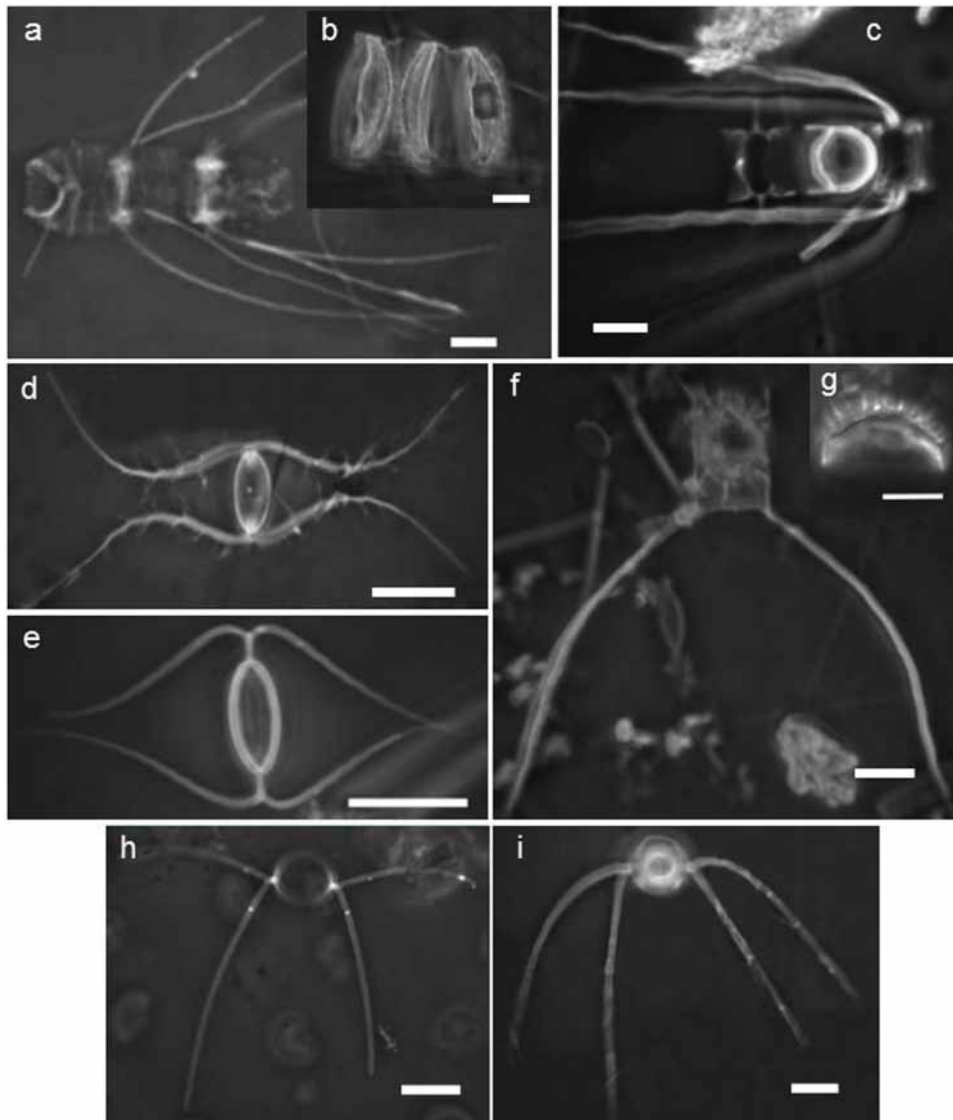


**Plate I.** Light microscope photographs of vegetative cells with their resting spores of some of the predominant *Chaetoceros* species in the sediment traps from the GoT. (a) Chain valves and (b) chain resting spores of *Chaetoceros costatus*. (c) Chain valves and resting spore of *Chaetoceros compressus*. (d) Valve of *Chaetoceros radicans* and (e) its resting spore. (f–g) Terminal valve and resting spore of *Chaetoceros affinis*. (h) Valve of *Chaetoceros curvisetus* and (i) its resting spore. The scale bar is 10  $\mu\text{m}$  in all images.

1996), *T. oestrupii* (Almaraz-Ruiz, 2017; Hasle and Syvertsen, 1997; Romero et al., 2009b; Sautter and Sancetta, 1992), *T. bacillare* (Sancetta, 1995), *T. nitzschioides* var. *parvum* (Almaraz-Ruiz, 2017; Schrader et al., 1993; Treppke et al., 1996), and *C. litoralis* (Lange and Syvertsen, 1989; Romero et al., 2009a, 2011). Therefore, in this study *T. bacillare*, *F. doliolus*, *T. nitzschioides* var. *parvum*, *C. litoralis*, and *T. oestrupii* were considered temperate to warm-water taxa. *Thalassiosira tenera* is reported as cosmopolitan, except for polar regions (Hasle and Syvertsen, 1997; Li et al., 2013; Naya, 2012) and *P. minus*, as a widely distributed species (Guiry and Guiry, 2020); since these taxa exhibited in our record a similar distribution to warm-water *N. pelagica*, *C. planetophorus*, *N. interruptestriata*, *T. lineata*, and *R. bergonii*, they were interpreted as such (Figure 4).

#### CONISS analysis

According to the abundance of the main diatom species and their ecological affinities based on the literature, three broad ecological assemblages were adopted: cold-water and high productivity taxa, temperate to warm-water taxa, and warm-water and low productivity taxa (Figure 4). These assemblages and the CONISS zonation are described below.

Visual observation of the CONISS and the broken stick model (Fig. S1) suggest four significant zones (at the 12.1 of total sum of squares) in the studied core (Figure 4). The classification on the first hierarchical level presents two significant diatom assemblage zones, the lower part of the core between ~1500 and ~1919 CE (32.5 to 11.5 cm), and the upper part between ~1920 and ~2014 CE (11.4 to 0 cm). The classification on the second level subdivides the lower part into two zones from ~1500 to ~1858 CE (32.5 cm to 16.6 cm) and ~1860 to ~1919 CE (16.5–11.5 cm). Finally, a third level separates another zone between ~1500 and ~1648 CE (32.5–28.0 cm).

The lowest zone (~1500 to ~1648 CE) was characterized by the predominance of cold-water and high productivity taxa (*T. nitzschioides*, *Chaetoceros* spores, *L. pacificum*, *T. nanolineata*, and *Rhizosolenia setigera*) and most temperate to warm-taxa (*T. nitzschioides* var. *parvum*, *C. litoralis*, and *T. oestrupii*). The zone from ~1650 to ~1858 CE showed a relative increase of the temperate to warm-taxa (*T. bacillare*, *F. doliolus*, *T. nitzschioides* var. *parvum*, and *C. litoralis*). From ~1860 to ~1919 CE some cold-water and high productivity taxa (*T. nitzschioides*, *Chaetoceros* spores, and *L. pacificum*) and most warm-water and low productivity diatoms (*N. pelagica*, *T. tenera*, and *R. bergonii*) increased. The upper part (~1920 to ~2014 CE) was characterized by high



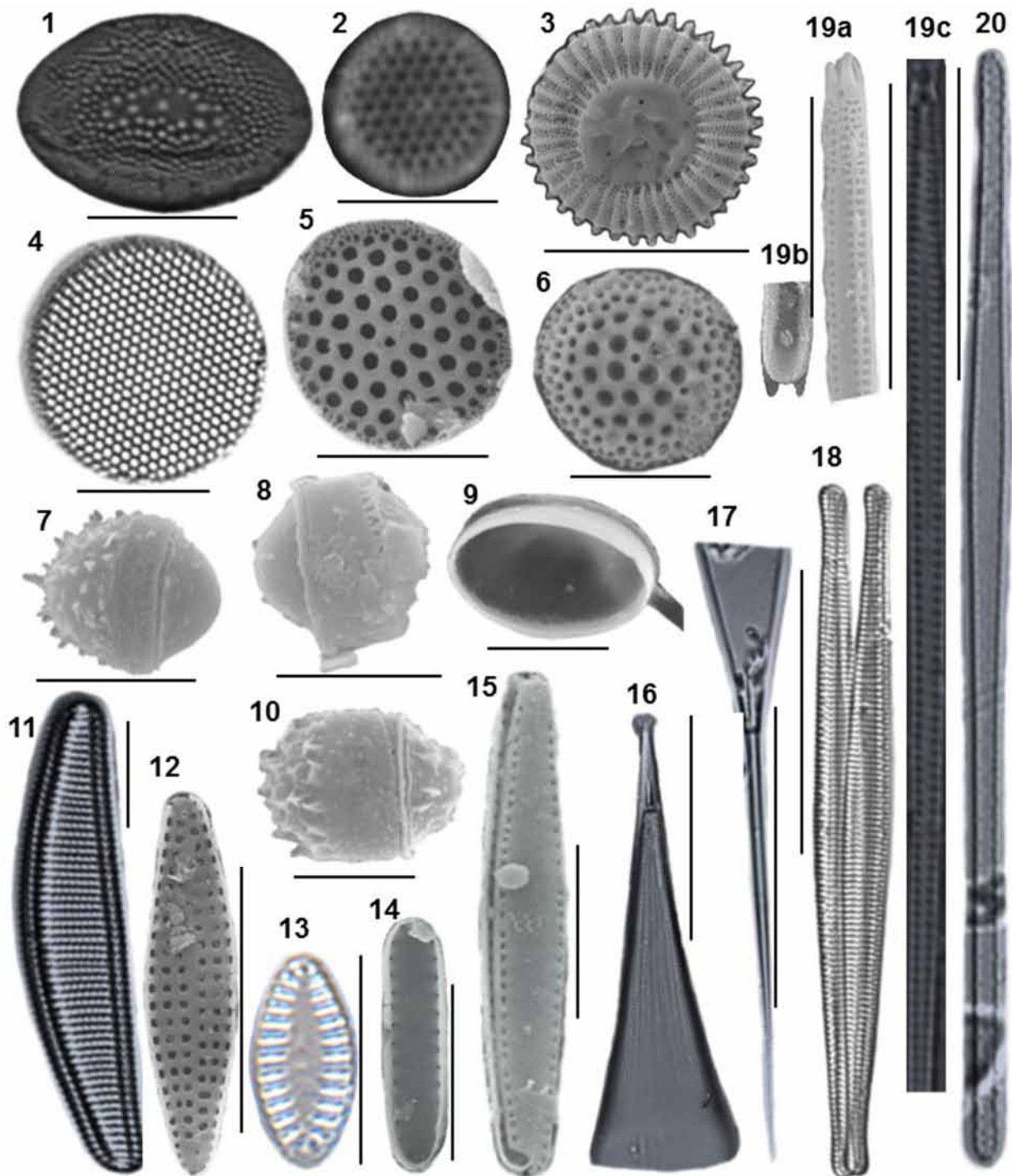


**Plate 2.** Scanning Electron Microscope (SEM) and Light Microscope (LM) images of the most abundant diatom taxa in the sediment core Tehua XII E03. (1) *Cymatodiscus planetophorus* (LM), (2) *Thalassiosira tenera* (LM), (3) *Cyclotella litoralis* (SEM), (4) *Thalassiosira lineata* (LM), (5) *Thalassiosira nanolineata* (SEM), (6) *Thalassiosira oestrupii* (SEM), (7) *Chaetoceros affinis* resting spore (SEM), (8) *Chaetoceros curvisetus* resting spore (SEM), (9) *Chaetoceros radicans* resting spore (internal view of the flat secondary valve, SEM), (10) *Chaetoceros costatus* resting spore (SEM), (11) *Fragillariopsis doliolus* (LM), (12) *Neodelphineis pelagica* (SEM), (13) *Plagiogramma minus* (LM), (14) *Thalassionema nitzschioides* var. *parvum* (SEM), (15) *Thalassionema nitzschioides* (SEM), (16) *Rhizosolenia bergonii* (LM), (17) *Rhizosolenia setigera* (LM), (18) *Nitzschia interruptestriata* (LM), (19) *Lioloma pacificum* (a-b in SEM, c in LM), and (20) *Thalassionema bacillare* (LM). Scale bar: 5  $\mu\text{m}$  in 7–10; 10  $\mu\text{m}$  in 1–6 and 11–15; 30  $\mu\text{m}$  in 16–18, and 20  $\mu\text{m}$  in 19a-c and 20.

abundances of all warm-water and low productivity taxa and almost all temperate to warm-water taxa (except *T. nitzschioides* var. *parvum*) (Figures 4 and 5).

## Discussion

### Chronology and sedimentation rate

The  $^{210}\text{Pb}$  dating is the most suitable method to obtain the chronology of recent sediments (~100 years) (Sanchez-Cabeza and

Ruiz-Fernández, 2012), whereas the  $^{14}\text{C}$  method is widely used to date sediments beyond the 1700–1800s (e.g. Choumiline et al., 2019; Gutiérrez et al., 2009; Staines-Urías et al., 2009). Although there are several palaeoceanographic studies in the GoT, these studies were focused on climate changes at the millennial scale and according to their reported ages they do not cover the last hundred years (e.g. Arellano-Torres et al., 2013; García-Gallardo et al., 2021; Hendy and Pedersen, 2006; Pichevin et al., 2010; Thunell and Kepple, 2004; Table 1). This is the first

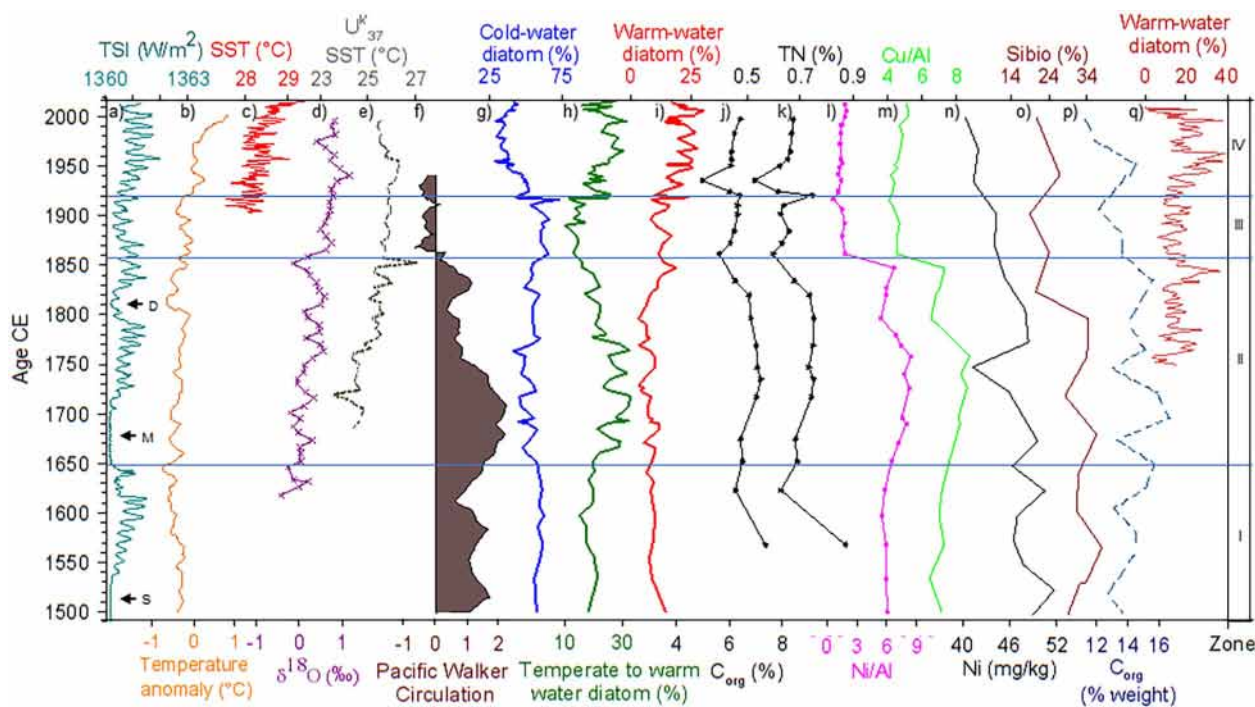


**Figure 5.** Paleoclimate records and the Tehua XII E03 record during the studied period. (a) Total Solar Irradiance (TSI,  $W/m^2$ ), Spörer (S), Maunder (M) and Dalton (D) minima (Lean, 2018). (b) Surface temperature anomaly ( $^{\circ}C$ ) from the Northern Hemisphere (Mann et al., 2009). (c) SST ( $^{\circ}C$ ) from GoT (IRI, 2015). (d) stratification of the water column (Staines-Urías et al., 2009) from Gulf of California. (e) Alkenone-derived SST ( $U_{37}^k$ ,  $^{\circ}C$ ) from Guaymas Basin (Goni et al., 2006). (f) Pacific Walker Circulation strength (Griffiths et al., 2016). (g) Cold-water diatom (%), (h) temperate-to-warm water diatom (%), (i) warm-water diatom (%), (j)  $C_{org}$  (%), (k) TN (%), (l) Ni/Al, and (m) Cu/Al from GoT (this study). (n) Ni concentration (mg/kg) (Choumiline et al., 2019) and (o) biogenic silica (Sibio %) (Barron and Bukry, 2007) from Gulf of California. (p)  $C_{org}$  (weight %) from off the Baja California margin (Juárez et al., 2014). (q) Warm-water diatom from Santa Barbara Basin (Barron et al., 2013). Horizontal lines indicate the periods (I to IV) identified with CONISS analysis.

high-resolution study in the region of the last ~500 years, where the environmental changes, linked to climatic variability, are based on an integrated  $^{210}Pb$ - $^{14}C$  age model.

A new  $^{14}C$  reservoir age ( $R=247 \pm 30$  years; Figure 3) was calculated for bulk sediments of the core Tehua XII E03 (section 2.2). This  $R$  value is higher than the reference reservoir age of the GoT proposed by Berger et al. (1966) ( $456 \pm 51$  years,  $R=18 + 50$  years), the marine reservoir effect applied by Thunell and Kepple (2004) (400 years), and Hendy and Pedersen (2006) (Table 1). Our reservoir age is consistent with the independently obtained  $^{210}Pb$  dates (Figure 2; Tables S1-S2), which are reliably validated by the Pu onset (Figure 2).

The method to estimate  $\Delta R$  has been used in sediment cores at Soledad Basin, Baja California, Mexico (Treinen-Crespo et al., 2021), where different  $\Delta R$ s are found for organic matter and planktonic foraminifera. This suggests that the reservoir age in *Turritella leverostoma* shell (Berger et al., 1966) cannot be used for bulk sediment. In recent and high-resolution sedimentary records (such as Tehua XII E03), it is essential to obtain reliable local reservoir corrections, as ages can be shifted by decades, or even centuries (Treinen-Crespo et al., 2021), thus invalidating the paleoreconstructions.

The sedimentation rate for the last century was  $0.14 \pm 0.07$  cm/year, within the range reported by Ruiz-Fernández et al. (2009) of 0.03–0.21 cm/year for the GoT. The sedimentation rate of  $0.08 \pm 0.04$  cm/year for the older sediments was similar to values obtained in previous studies in GoT for the late-Holocene of ~0.1 cm/yr (Table 1) (Arellano-Torres et al., 2013; Blanchet et al., 2012; García-Gallardo et al., 2021; Hendy and Pedersen, 2006; Thunell and Kepple, 2004).

#### Origin of organic matter in the Tehua XII E03

The origin of sedimentary organic matter was inferred through the C:N ratio and  $\delta^{13}C$  that indicate the relative contributions of

organic matter from different sources (Lamb et al., 2006). Typically, C:N ratio values above 12 and  $\delta^{13}C$  values that range from  $-33$  to  $-25$  ‰ suggest the predominance of terrestrial organic matter. C:N ratio values between 4 and 10, and  $\delta^{13}C$  values ranging from  $-21$  to  $-18$  ‰ indicate a marine origin (Lamb et al., 2006). Thus, our values of C:N ratio (~9) and  $\delta^{13}C$  (~-22 to ~-18 ‰) suggest that the organic matter preserved in the GoT sediments is predominantly of marine origin (Figure 4; Table S3).

#### Productivity variation in the Gulf of Tehuantepec over the last five centuries

The diatom abundance and geochemical proxies used in this study ( $C_{org}$ , TN,  $\delta^{13}C$ , Ni/Al, and Cu/Al) suggest relative productivity changes related to LIA and CWP conditions during the last five centuries. According to CONISS analysis, four significant zones were recognized within these two conditions (Figure 4). These periods are compared below (Figure 5) with solar irradiance (Lean, 2018), temperature records (Goni et al., 2006; Mann et al., 2009; Staines-Urías et al., 2009), and the Pacific Walker Circulation strength through the Southern Oscillation Index (SOI) (Griffiths et al., 2016). Also, we compared our record with other ETNP exported productivity records (Barron and Bukry, 2007; Barron et al., 2013; Choumiline et al., 2019; Juárez et al., 2014).

**Little Ice Age (zone I ~1500 to ~1648 CE and zone II ~1650 to ~1858 CE).** During the LIA period, the predominance of cold-water and high productivity assemblage and the low abundance of temperate to warm-water and warm-water taxa, as well as the highest values of  $C_{org}$ , TN, Ni/Al, and Cu/Al (Figures 4 and 5), overall suggest the presence of upwelling and high productivity, presumably linked to LIA. Similar findings are observed in the Gulf of California and Baja California margin records during the

LIA (Barron and Bukry, 2007; Barron et al., 2003; Choumiline et al., 2019; Juárez et al., 2014; Figure 5).

The LIA in the Northern Hemisphere has often been observed as negative surface temperature anomalies ( $\sim -0.7$  to  $\sim -0.3^\circ\text{C}$ , Mann et al., 2009), associated with lower solar irradiance (Bard et al., 2000; Lean, 2018). Under these conditions, the mean position of the ITCZ is displaced southward (Griffiths et al., 2016; Haug et al., 2001; Sachs et al., 2009) related with a strengthened Pacific Walker Circulation (Griffiths et al., 2016). Although during the LIA, presumably, La Niña-like conditions were predominant (Beaufort and Grelaud, 2017; Griffiths et al., 2016; Yan et al., 2011), as it is suggested by the SOI (Figure 5, Griffiths et al., 2016), the temporal resolution of our samples does not allow direct comparison with ENSO variability.

The southern position of the ITCZ reinforced northeasterly trade winds into the Gulf of Mexico and the Caribbean Sea (Black et al., 1999; Nyberg et al., 2002), which reached the Pacific coast of Central America (Glynn et al., 1983) and the GoT. Also, a southward migration of the high-pressure systems may have resulted in more frequent outbreaks, particularly during winters (Lozano-García Mdel et al., 2007; Nyberg et al., 2002). As a result, strong Tehuanos winds blowing during the LIA, likely enhanced mixing and upwelling and therefore caused high productivity due to the nutrient input from subsurface waters into the photic zone (Lluch-Cota et al., 1997; Pennington et al., 2006). In the Gulf of Papagayo, close to the GoT, Glynn et al. (1983) reported the demise of coral reefs likely caused by low SST, triggered by an increase in duration or intensity of seasonal upwelling during the LIA ( $\sim 1600$  to  $\sim 1900$  CE).

Our diatom record suggests that the LIA was not a homogeneous cold period. The increased abundance of the temperate to warm-water assemblage (Figure 4) suggests less cold and less productive conditions from  $\sim 1650$  to  $\sim 1858$  CE (zone II), although our geochemical productivity proxies in this interval show a slight decrease after  $\sim 1850$ , similar to those found in the Gulf of California (biogenic silica %, Barron and Bukry, 2007) and the Baja California margin ( $C_{\text{org}}$ , Juárez et al., 2014) (Figure 5).

The relative decrease in productivity suggested by our diatom record between  $\sim 1650$  and  $\sim 1858$  CE is associated with the increase in solar irradiance after the Maunder minimum and the decrease in Pacific Walker Circulation (Figure 5). Other studies in the ETNP have also indicated the heterogeneity of the LIA, also attributed to solar activity variations (Barron and Bukry, 2007; Barron et al., 2003; Choumiline et al., 2019; Cuna et al., 2014; Lozano-García Mdel et al., 2007; Rodríguez-Ramírez et al., 2015; Staines-Urías et al., 2009).

**Transition period (zone III  $\sim 1860$  to  $\sim 1919$  CE).** Although there is still no consensus in the ETNP records about the end of the LIA, we identified a transition period from  $\sim 1860$  to  $\sim 1919$  CE that could be interpreted as the end of LIA and the beginning of the CWP. The records closest to the GoT report the end of LIA at about  $\sim 1750$  CE (Ricaurte-Villota et al., 2013),  $\sim 1820$  CE (Juárez et al., 2014),  $\sim 1850$  CE (Barron and Bukry, 2007; Barron et al., 2003; Choumiline et al., 2019; Cuna et al., 2014; Del Castillo-Batista et al., 2018), and even  $\sim 1900$  (Hodell et al., 2005).

In this interval, though some cold-water and high productivity taxa (*Chaetoceros* spores, *T. nitzschioides*, and *L. pacificum*) remained abundant, the increased abundance of warm-water and low productivity taxa (*N. pelagica*, *T. tenera*, and *R. bergonii*) characterized the period, indicating the transition toward warmer and less productive conditions (Figure 4). Likewise, the sediments from this period were characterized by lower values of  $C_{\text{org}}$ , TN, Ni/Al, and Cu/Al ratio, suggesting a reduction in the productivity of the GoT, similarly to some productivity proxies from Gulf of California and off the Baja California margin (Barron and

Bukry, 2007; Barron et al., 2003; Choumiline et al., 2019; Juárez et al., 2014; Figure 5).

As mentioned in section 3.4, *R. bergonii* is a deep-dwelling taxon that indicates strong stratification in the water column (Baumgartner et al., 1985; Kemp et al., 2000; Lange et al., 1987, 1994; Romero et al., 2011). In the GoT, greater stratification occurs during the summer and autumn when the thermocline and nutricline are found beyond  $\sim 50$  m ( $\sim 30$  m during winter), and the upwelling and mixing events are restricted (Lluch-Cota et al., 1997). Also, this taxon is common during El Niño events on the Eastern North Pacific coast. Thus, the increased abundance of *R. bergonii* suggests that the GoT water column became more stratified around the mid-1800s, similar to the findings of Staines-Urías et al. (2009) (Figure 4).

The general trend of this period shows a progressive warming since  $\sim 1850$  CE (IPCC, 2014) largely associated with solar irradiance (Bard et al., 2000; Hoyt and Schatten, 1993; Lean et al., 1995) and global warming (IPCC, 2014). This warming trend is also observed in the Gulf of California by Staines-Urías et al. (2009), who pointed out rapid warming since the mid-1800s and enhanced water column stratification. Also, Goni et al. (2006) found a general trend of increased SST of  $1$ – $2^\circ\text{C}$  in Guaymas and Cariaco Basins since  $\sim 1800$  CE (Figure 5) and related them to the end of the LIA. Likewise, this period coincides with the weakening of the Pacific Walker Circulation since  $\sim 1860$  CE (Griffiths et al., 2016; Yan et al., 2011) and the northward migration of the ITCZ (Sachs et al., 2009). Lacustrine sediments from central Mexico recorded wetter conditions after the LIA, coinciding with the ITCZ's northward displacement (Cuna et al., 2014). These conditions probably led to a weakening of the northeasterly trade winds over the Caribbean Sea (Nyberg et al., 2002), as well as to lesser frequent polar outbreaks over the Gulf of Mexico (Lozano-García Mdel et al., 2007), which would result in weaker Tehuanos winds in the GoT and consequently less upwelling and lower productivity. These findings together with those reported in the northwestern region of Mexico suggest warmer climate conditions and a likely decline in productivity during this transitional period in the ETNP.

**Current warm period (zone IV  $\sim 1920$  CE to  $\sim$ today).** The most recent period is characterized by the highest abundance of the warm-water and oligotrophic assemblage together with a high abundance of moderate to warm conditions taxa (Figure 4). High abundances of *N. interruptestriata*, *T. nitzschioides* var. *parvum*, and *F. doliolus* have been interpreted in La Paz, to reflect an incursion of tropical/subtropical water during anomalously warm periods (Acevedo-Acosta et al., 2021). Also, the rapid increase up to  $\sim 7.4\%$  of the *C. planetophorus* (Figure 4), a tropical taxon commonly found at temperatures above  $23.3^\circ\text{C}$  in the northwestern coasts of Mexico (Estrada Gutiérrez et al., 2022), supports the idea that warmer conditions prevailed during this period. Diatom sedimentary records (Barron and Bukry, 2007; Barron et al., 2013; Esparza-Alvarez et al., 2007; Martínez-López et al., 2007) and planktonic foraminifera (Field et al., 2006) from the Eastern North Pacific also showed evidence of the global warming trend. For example, the percentage of warm-water diatoms (and silico-flagellates, not graphed in Figure 5) from Santa Barbara Basin exhibited a clear increase since  $\sim 1920$  CE (Barron et al., 2013), in agreement with the peak of Alkenone-derived SST ( $U_{37}^k$ ) from the Guaymas Basin during the same time (Goni et al., 2006) (Figure 5). Goni et al. (2006) attributed this increase in  $U_{37}^k$  SST to the northernmost Subtropical High and ITCZ migration in response to the Northern Hemisphere insolation. Under boreal summer conditions, the atmospheric regime results in weak winds over the central and southern regions of the Gulf of California; consequently, upwelling shuts down, leading to progressive

warming and thermal stratification in the Guaymas Basin. In addition, the  $U^k_{37}$  SST peak after ~1920 CE could also reflect the northernmost incursion of warmer tropical water in the Eastern Tropical Pacific, similar to El Niño conditions in this region (e.g. Lavín et al., 1997).

On the other hand, our  $C_{org}$ , TN, Ni/Al, and Cu/Al records also remain with low values (Figures 4 and 5; Table S6). Similarly, geochemical productivity proxies from the Gulf of California indicated reduced productivity in this period (Barron and Bukry, 2007; Choumiline et al., 2019; Juárez et al., 2014; Figure 5). In the GoT, human impact contamination has been identified by the increase in trace metals in the coastal and shelf zones (Pica-Granados et al., 1994; Ruiz-Fernández et al., 2004); however, since our sedimentary record is further seaward and deeper, our Ni and Cu concentrations were lower (16.8 mg/kg for Ni and 47.0 mg/kg for Cu) than in the coastal and shelf zones. Therefore, we considered that our Ni and Cu records are not masked by human impact. Also, these elements' trend has been decreasing since ~1860 CE (together with those of the other productivity proxies) before the anthropic influence was evident (~1980) in the region (Ruiz-Fernández et al., 2004).

During this period, a generalized warming trend is observed in diverse records (IPCC, 2014; Mann et al., 2009), including the Eastern North Pacific (Barron et al., 2013; Goni et al., 2006; Staines-Urías et al., 2009). In the SST record of the GoT, the evident warming trend of surface water in the 20th century (IRI, 2015) (Figure 5) leads us to infer that the reduced productivity during the CWP is associated with the warming trend, which caused a sharp upper ocean stratification, as is observed in the  $\delta^{18}O$  of the planktonic foraminiferal record from the Gulf of California (Staines-Urías et al., 2009; Figure 5).

Our observations document the dominance of warm conditions and low productivity since ~1920 CE in a more tropical area (~15°N latitude). These results agree with previous studies further north; therefore, this study documented the regional scale of the warming trend and its consequence on productivity in the tropical oceans.

## Conclusions

This study provides a new  $\Delta R = 247 \pm 30$  years for the last 500 years in the Gulf of Tehuantepec, estimated through the combinations of  $^{210}Pb$  and  $^{14}C$  methods in a bayesian model.

The diatom and geochemical proxies analyzed in the Gulf of Tehuantepec sediments reflected two predominant productivity conditions during the last five centuries, higher productivity conditions during the Little Ice Age and lesser productivity conditions during the Current Warm Period.

During the part of the LIA found in our record, low solar irradiance (Spörer, Maunder and Dalton minima) promoted the southward migration of the Intertropical Convergence Zone, which likely promoted more Tehuanos winds in the Gulf of Tehuantepec. This scenario resulted in enhanced upwelling and higher productivity as evidenced by the prevalence of cold and high productivity taxa (*Chaetoceros* spores, *T. nitzschioides*, *L. pacificum*, *T. nanolineata*, and *R. setigera*) and high values of  $C_{org}$ , TN, Ni/Al, and Cu/Al. Temperate conditions and lesser productivity from ~1650 to ~1858 CE, were suggested by the increase of some temperate to warm-water taxa (*T. bacillare*, *T. nitzschioides* var. *parvum*, *F. doliolus*, and *T. lineata*).

A transitional period (~1860 to ~1919 CE) toward the Current Warm Period was indicated by the appearance of most warm-water taxa (*N. pelagica*, *T. tenera*, and *R. bergonii*) as well as lower values of  $C_{org}$ , TN, Ni/Al, and Cu/Al. From ~1920 to ~2014 CE, the dominance of temperate to warm-water and mainly warm-water taxa (*T. bacillare*, *F. doliolus*, *C. litoralis*, *T. oestrupii*, *N. pelagica*, *C. planetophorus*, *T. tenera*, *P. minus*, *N. interruptestriata*, *T. lineata*, and *R. bergonii*) and low values of

geochemical productivity proxies indicated even warmer conditions and lower productivity. These conditions were associated with diminished upwelling, and probably increased upper water column stratification and deeper thermocline derived from prevalence of warming trend, the northward migration of the ITCZ and weakening of the Pacific Walker Circulation.

Our findings highlight the importance of high-resolution productivity reconstructions and contribute to the knowledge of the response of the tropical regions to the Little Ice Age and Current Warm Period climates.

## Acknowledgements

We thank the crew of the R/V “El Puma” for their assistance during the TEHUA XII expedition and core collection. Libia Hascibe Pérez Bernal performed the radiometric analysis for  $^{210}Pb$  dating. Laura Elena Gómez-Lizárraga provided technical aid with the SEM images at the ICML, UNAM. We are also indebted to anonymous reviewers for their valuable suggestions to improve this paper.

## Funding

The author(s) disclosed receipt of the following financial support for the research, authorship, and/or publication of this article: Financial support for the development of this project and publication costs was provided by the Instituto de Ciencias del Mar y Limnología, UNAM. Support for field sampling was provided by the UNAM through oceanographic mission TEHUA XII. The first author (LAR) thanks the Graduate Program in Marine Science and Limnology at UNAM, Mexico, and the financial support provided by the National Council of Science and Technology (CONACYT) for the doctoral scholarship (Grant number: 556646), as well as the Institut de Recherche pour le Développement (IRD) for the fellowship grant for an academic stay at the Laboratory of Oceanography and Climate (LOCEAN), IRD France-Nord. Also, the authors are grateful to the ALYSES platform for their support for carbon and nitrogen analyses.

## ORCID iDs

María Luisa Machain-Castillo  <https://orcid.org/0000-0002-4973-4967>

Alejandro Rodríguez-Ramírez  <https://orcid.org/0000-0003-1605-5471>

## Supplemental material

Supplemental material for this article is available online.

## References

- Acevedo-Acosta JD, Martínez-López A, Morales-Acoltzi T et al. (2021) Self-organization maps (SOM) in the definition of a “transfer function” for a diatoms-based climate proxy. *Climate Dynamics* 56(1-2): 423–437.
- Almaraz-Ruiz L (2017) *Variabilidad de las surgencias en el golfo de Tehuantepec durante el último siglo a través del registro sedimentario de diatomeas y foraminíferos bentónicos*. MSc thesis, Universidad Nacional Autónoma de México.
- Amador JA, Alfaro EJ, Lizano OG et al. (2006) Atmospheric forcing of the eastern tropical Pacific: A review. *Progress in Oceanography* 69(2-4): 101–142.
- Aquino-López MA, Blaauw M, Christen JA et al. (2018) Bayesian analysis of  $^{210}Pb$  dating. *Journal of Agricultural Biological and Environmental Statistics* 23(3): 317–333.
- Aquino-López MA, Ruiz-Fernández AC, Blaauw M et al. (2020) Comparing classical and Bayesian  $^{210}Pb$  dating models in human-impacted aquatic environments. *Quaternary Geochronology* 60, 101106.

- Arellano-Torres E, Machain-Castillo ML, Contreras-Rosales LA et al. (2013) Foraminiferal faunal evidence for glacial–interglacial variations in the ocean circulation and the upwelling of the Gulf of Tehuantepec (Mexico). *Marine Micropaleontology* 100: 52–66.
- Bard E, Raisbeck G, Yiou F et al. (2000) Solar irradiance during the last 1200 years based on cosmogenic nuclides. *Tellus, Series B: Chemical and Physical Meteorology* 52(3): 985–992.
- Barron JA and Bukry D (2007) Solar forcing of Gulf of California climate during the past 2000 yr suggested by diatoms and silicoflagellates. *Marine Micropaleontology* 62(2): 115–139.
- Barron JA, Bukry D and Bischoff JL (2003) A 2000-yr-long record of climate from the Gulf of California. In: West NL and Blomquist GJ (eds) *Proceedings of the Nineteenth Pacific Climate Workshop*. Asilomar, Pacific Grove, CA, pp.1–15.
- Barron JA, Bukry D and Bischoff JL (2004) High resolution Paleooceanography of the Guaymas Basin, Gulf of California, during the past 15 000 years. *Marine Micropaleontology* 50(3-4): 185–207.
- Barron JA, Bukry D and Dean WE (2005) Paleooceanographic history of the Guaymas Basin, Gulf of California, during the past 15,000 years based on diatoms, silicoflagellates, and biogenic sediments. *Marine Micropaleontology* 56(3-4): 81–102.
- Barron JA, Bukry D and Field D (2010) Santa Barbara Basin diatom and silicoflagellate response to global climate anomalies during the past 2200 years. *Quaternary International* 215(1-2): 34–44.
- Barron JA, Bukry D, Field DB et al. (2013) Response of diatoms and silicoflagellates to climate change and warming in the California current during the past 250 years and the recent rise of the toxic diatom *Pseudo-nitzschia australis*. *Quaternary International* 310: 140–154.
- Baumgartner T, Ferreira-Bartrina V, Schrader H et al. (1985) A 20-year varve record of siliceous phytoplankton variability in the central Gulf of California. *Marine Geology* 64(1-2): 113–129.
- Beaufort L and Grelaud M (2017) A 2700-year record of ENSO and PDO variability from the californian margin based on coccolithophore assemblages and calcification. *Progress in Earth and Planetary Science* 4(1), 5.
- Bennett KD (1996) Determination of the number of zones in a biostratigraphical sequence. *New Phytologist* 132(1): 155–170.
- Berger R, Taylor RE and Libby WF (1966) Radiocarbon content of marine shells from the California and Mexican West coast. *Science* 153(3738): 864–866.
- Blaauw M (2022) Package “IntCal”. Radiocarbon Calibration Curves. *CRAN* 28.
- Blaauw M and Christen JA (2011) Flexible paleoclimate age-depth models using an autoregressive gamma process. *Bayesian Analysis* 6(3): 457–474.
- Blaauw M, Christen JA, Aquino-Lopez MA et al. (2021) Package “rplum”. Bayesian Age-Depth Modelling of Cores Dated by Pb-210. *CRAN* 12.
- Blaauw M, Christen JA, Aquino-Lopez MA et al. (2022) Package “rbacon”. Age-Depth Modelling using Bayesian Statistics. *CRAN* 53.
- Black DE, Peterson LC, Overpeck JT et al. (1999) Eight centuries of North Atlantic Ocean atmosphere variability. *Science* 286(5445): 1709–1713.
- Blanchet CL, Kasten S, Vidal L et al. (2012) Influence of diagenesis on the stable isotopic composition of biogenic carbonates from the Gulf of Tehuantepec oxygen minimum zone. *Geochemistry, Geophysics, Geosystems* 13(4): 1–20.
- Calvert SE and Pedersen TF (2007) Chapter fourteen elemental proxies for Palaeoclimatic and palaeoceanographic variability in marine sediments: Interpretation and Application. *Developments in Marine Geology* 1(07): 567–644.
- Choumiline K, Pérez-Cruz L, Gray AB et al. (2019) Scenarios of deoxygenation of the eastern tropical North Pacific during the past millennium as a window into the future of oxygen minimum zones. *Frontiers in Earth Science* 7: 1–23.
- Crosta X and Koc N (2007) Diatoms: From micropaleontology to isotope geochemistry. *Developments in Marine Geology* 1: 327–369.
- Crowley TJ, Zielinski G, Vinther B et al. (2008) Volcanism and the little ice age. *PAGES news* 16(2): 22–23.
- Cuna E, Zawisza E, Caballero M et al. (2014) Environmental impacts of Little Ice Age cooling in central Mexico recorded in the sediments of a tropical alpine lake. *Journal of Paleolimnology* 51(1): 1–14.
- Cupp EE (1943) Marine plankton diatoms of the west coast of North America. *Bulletin of The Scripps Institution of Oceanography* 5(1): 1–238.
- Del Castillo-Batista AP, Figueroa-Rangel BL, Lozano-García S et al. (2018) 1580 years of human impact and climate change on the dynamics of a *Pinus-Quercus-Abies* forest in west-central Mexico. *Revista Mexicana de Biodiversidad* 89(1): 208–225.
- Díaz-Asencio M, Sanchez-Cabeza JA, Ruiz-Fernández AC et al. (2020) Calibration and use of well-type germanium detectors for low-level gamma-ray spectrometry of sediments using a semi-empirical method. *Journal of Environmental Radioactivity* 225: 106385.
- Esparza-Alvarez MA, Herguera JC and Lange C (2007) Last century patterns of sea surface temperatures and diatom (>38 µm) variability in the Southern California Current. *Marine Micropaleontology* 64(1-2): 18–35.
- Estrada Gutiérrez KM, Hernández Almeida OU, Siqueiros Beltrones DA et al. (2022) First record of *Cymatodiscus planetophorus* (Bacillariophyta) for littorals of NW Mexico; ecological remarks. *Revista Bio Ciencias* 9(322): 1–13.
- Fiedler PC and Talley LD (2006) Hydrography of the eastern tropical Pacific: A review. *Progress in Oceanography* 69(2-4): 143–180.
- Field DB, Baumgartner TR, Charles CD et al. (2006) Planktonic Foraminifera of the California current reflect 20th-Century warming. *Science Translational Medicine* 311(5757): 63–66.
- García-Gallardo Á, Machain-Castillo ML and Almaraz-Ruiz L (2021) Paleooceanographic evolution of the Gulf of Tehuantepec (Mexican Pacific) during the last ~6 millennia. *The Holocene* 31(4): 529–544.
- Gibson KA, Thunell RC, Machain-Castillo ML, Fehrenbacher J, Spero HJ, Wejnert K, Nava-Fernández X, and Tappa EJ (2016) Evaluating controls on planktonic foraminiferal geochemistry in the Eastern Tropical North Pacific. *Earth and Planetary Science Letters*. Elsevier B.V. 452: 90–103.
- Glynn PW, Druffel EM and Dunbar RB (1983) A dead Central American coral reef tract: possible link with the Little Ice Age. *Journal of Marine Research* 41(3): 605–637.
- Goni MA, Thunell RC, Woodworth MP et al. (2006) Changes in wind-driven upwelling during the last three centuries: Inter-ocean teleconnections. *Geophysical Research Letters* 33(15): 3–6.
- Goodfriend GA and Flessa KW (1997) Radiocarbon reservoir ages in the Gulf of California: Roles of upwelling and flow from the Colorado river. *Radiocarbon* 39(2): 139–148.
- Griffiths ML, Kimbrough AK, Gagan MK et al. (2016) Western Pacific hydroclimate linked to global climate variability over the past two millennia. *Nature Communications* 7: 1–9.
- Grimm EC (1987) CONISS: A FORTRAN 77 program for stratigraphically constrained cluster analysis by the method of incremental sum of squares. *Computational Geosciences* 13: 13–35.
- Guiry MD and Guiry G (2020) *AlgaeBase*. World-wide electronic publication, National University of Ireland, Galway. Available at: <https://www.algaebase.org> (accessed 9 January 2022).

- Gutiérrez D, Sifeddine A, Field DB et al. (2009) Rapid reorganization in ocean biogeochemistry off Peru towards the end of the Little Ice Age. *Biogeosciences* 6(5): 835–848.
- Hasle GR and Syvertsen EE (1997) Marine diatoms. In: Tomas CR (ed.) *Identifying Marine Diatoms*. San Diego, CA: Academic Press, pp.5–386.
- Haug GH, Hughen KA, Sigman DM et al. (2001) Southward migration of the Intertropical Convergence Zone through the holocene. *Science* 293(5533): 1304–1308.
- Heaton TJ, Köhler P, Butzin M et al. (2020) Marine20—The marine radiocarbon age calibration curve (0–55,000 cal BP). *Radiocarbon* 62(4): 779–820.
- Hendy IL and Pedersen TF (2006) Oxygen minimum zone expansion in the Eastern Tropical North Pacific during deglaciation. *Geophysical Research Letters* 33(20): 1–5.
- Hernández-Becerril DU, Barón-Campis SA, Ceballos-Corona JGA et al. (2021) Catálogo de fitoplancton del Pacífico central mexicano, Cruceros “MareaR” (2009–2019). B/O “El Puma.” *Universidad Nacional Autónoma de México*. México: Universidad Nacional Autónoma de México.
- Hodell DA, Brenner M, Curtis JH et al. (2005) Climate change on the Yucatan Peninsula during the Little Ice Age. *Quaternary Research* 63(2): 109–121.
- Hoyt DV and Schatten KH (1993) A discussion of plausible solar irradiance variations, 1700–1992. *Journal of Geophysical Research Space Physics* 98(A11): 18895–18906.
- IPCC (2014) *Climate Change 2014: Synthesis Report. Contribution of Working groups I, II and III to the Fifth Assessment Report of the Intergovernmental Panel on Climate Change*. In: Pachauri LA and Meyer RK. Geneva, Switzerland.
- IRI (2015) *Dataset GOSTA gisst22 sst*. Available at: <http://iridl.ldeo.columbia.edu/SOURCES/GOSTA/gisst22/sst/Y/%2815.66N%29%2815.66N%29RANGEEDGES/X/%2895.32W%29%2895.32W%29RANGEEDGES/> (accessed 17 August 2021).
- Juárez M, Sánchez A and González-Yajimovich O (2014) Variabilidad de la productividad biológica marina en el Pacífico nororiental durante el último milenio. *Ciencias Marinas* 40(4): 211–220.
- Juggins S (2020) The Rioja package. *Analysis of Quaternary Science Data* 54: 1–53.
- Kemp AES, Pike J, Pearce RB et al. (2000) The “Fall dump” — a new perspective on the role of a “shade flora” in the annual cycle of diatom production and export flux. *Deep-Sea Research Part II: Topical Studies in Oceanography* 47(9–11): 2129–2154.
- Kessler WS (2006) The circulation of the eastern tropical Pacific: A review. *Progress in Oceanography* 69(2–4): 181–217.
- Lamb AL, Wilson GP and Leng MJ (2006) A review of coastal palaeoclimate and relative sea-level reconstructions using  $\delta^{13}C$  and C/N ratios in organic material. *Earth-Science Reviews* 75(1–4): 29–57.
- Lange CB, Berger WH, Burke SK et al. (1987) El Niño in Santa Barbara Basin: Diatom, radiolarian and foraminiferan responses to the “1983 El Niño” event. *Marine Geology* 78(1–2): 153–160.
- Lange CB, Burke SK and Berger WH (1990) Biological production off Southern California is linked to climatic change. *Climatic Change* 16: 319–329.
- Lange CB and Syvertsen EE (1989) *Cyclotella litoralis* sp. nov. (Bacillariophyceae), and its relationship to *C. striata* and *C. stylorum*. *Nova Hedwigia* 48(3–4): 341–356.
- Lange CB, Treppke UF and Fischer G (1994) Seasonal diatom fluxes in the Guinea Basin and their relationships to trade winds, hydrography and upwelling events. *Deep-Sea Research Part I* 41: 5–6.
- Lange CB, Weinheimer AL, Reid FMH et al. (1997) Sedimentation patterns of diatoms, radiolarians, and silicoflagellates in Santa Barbara Basin, California. *California Cooperative Oceanic Fisheries Investigations Reports* 38(August 1993): 161–170.
- Lavín MF, Beier E and Badan A (1997) Estructuras hidrográficas y circulación del Golfo de California: Escalas estacional e interanual, Contribuciones a la Oceanografía Física en México. *Monografía* 3: 141–171.
- Lavín MF, Fiedler PC, Amador JA et al. (2006) A review of eastern tropical Pacific oceanography: Summary. *Progress in Oceanography* 69(2–4): 391–398.
- Lean J, Beer J and Bradley R (1995) Reconstruction of solar irradiance since 1610: Implications for climate change. *Geophysical Research Letters* 22(23): 3195–3198.
- Lean JL (2018) Estimating solar irradiance since 850 CE. *Earth and Space Science* 5(4): 133–149.
- Li G, Cheng L, Zhu J et al. (2020) Increasing ocean stratification over the past half-century. *Nature Climate Change* 10(12): 1116–1123.
- Li Y, Zhao Q and Lü S (2013) The genus *Thalassiosira* off the Guangdong coast, South China Sea. *Botanica Marina* 56(1): 83–110.
- Lluch-Cota SE, Álvarez-Borrego S, Santamaría-ángel E et al. (1997) The Gulf of Tehuantepec and adjacent areas: Spatial and temporal variation of satellite-derived photosynthetic pigments. *Ciencias Marinas* 23(3): 329–340.
- Lozano-García Mdel S, Caballero M, Ortega B et al. (2007) Tracing the effects of the Little Ice Age in the tropical lowlands of eastern Mesoamerica. *Proceedings of the National Academy of Sciences of the United States of America* 104(41): 16200–16203.
- Machain-Castillo ML, Monreal-Gómez MA, Arellano-Torres E et al. (2008) Recent planktonic foraminiferal distribution patterns and their relation to hydrographic conditions of the Gulf of Tehuantepec, Mexican Pacific. *Marine Micropaleontology* 66(2): 103–119.
- Mann ME, Zhang Z, Rutherford S et al. (2009) Global signatures and dynamical origins of the Little Ice Age and medieval climate anomaly. *Science* 326(5957): 1256–1260.
- Martínez-López A, Baumgartner TR and Lange C (2007) Effects of Climate Change on Production of Siliceous Phytoplankton Over the Twentieth Century as Recorded in Sediments of the Santa Barbara Basin off Southern California. In: *Proceedings of the American Geophysical Union 2007 Joint Assembly*, pp.1–2.
- Meave del Castillo MA and Hernández-Becerril DU (1998) Fitoplancton. In: Tapia-García M (ed.) *El Golfo de Tehuantepec: El Ecosistema y Sus Recursos*. México, D. F.: Universidad Autónoma Metropolitana (Unidad Iztapalapa), pp.59–74.
- Meave del Castillo ME (2002) *Diatomeas planctónicas del Océano Pacífico de México. Informe final SNIB-CONABIO proyecto No. H176*. México, D. F.
- Miller GH, Geirsdóttir Á, Zhong Y et al. (2012) Abrupt onset of the Little Ice Age triggered by volcanism and sustained by sea-ice/ocean feedbacks. *Geophysical Research Letters* 39(2): 1–5.
- Moreno JL, Licea S and Santoyo H (1996) *Diatomeas Del Golfo de California*. Universidad Autónoma de Baja California Sur. México: La Páz.
- Moreno-Ruiz JL, Tapia-García M, Licea S et al. (2011) Ecological composition and distribution of the diatoms from the Laguna Superior, Oaxaca, Mexico. *Journal of environmental biology* 32(4): 425–442.
- Naya T (2012) Marine *Thalassiosira* species from coastal pleistocene sediments in central Kanto Plain, Japan. *Diatom Research* 27(3): 141–163.
- Nyberg J, Malmgren BA, Kuijpers A et al. (2002) A centennial-scale variability of tropical North Atlantic surface hydrography during the late holocene. *Palaeogeography Palaeoclimatology Palaeoecology* 183(1–2): 25–41.

- Oksanen J, Blanchet FG, Friendly M et al. (2020) Vegan-package Community Ecology Package: Ordination, Diversity and Dissimilarities, p.298.
- Pennington JT, Mahoney KL, Kuwahara VS et al. (2006) Primary production in the eastern tropical Pacific: A review. *Progress in Oceanography* 69(2-4): 285–317.
- Pica-Granados Y, Botello AV and Villanueva SF (1994) *La contaminación por actividades petroleras en el Puerto de Salina Cruz Oaxaca (1990–199)*. Serie Grandes Temas de la Hidrobiología: vol. 2. Los sistemas litorales. Mexico City: UAMI, UNAM.
- Pichevin LE, Ganeshram RS, Francavilla S et al. (2010) Inter-hemispheric leakage of isotopically heavy nitrate in the eastern tropical Pacific during the last glacial period. *Paleoceanography* 25, PA1204.
- R Core Team (2021) *R: A language and environment for statistical computing*. R Foundation for Statistical Computing, Vienna, Austria. Available at: <https://www.r-project.org/>. (accessed 7 January 2022).
- Reimer RW and Reimer PJ (2017) An online application for  $\delta r$  Calculation. *Radiocarbon* 59(5): 1623–1627.
- Ren J, Gersonde R, Esper O et al. (2014) Diatom distributions in northern North Pacific surface sediments and their relationship to modern environmental variables. *Palaeogeography Palaeoclimatology Palaeoecology* 402: 81–103.
- Ricaurte-Villota C, González-Yajimovich O and Sanchez A (2013) Coupled response of rainfall and denitrification to solar forcing during the holocene in Alfonso Basin. *Ciencias Marinas* 39(2): 151–164.
- Rines JEB and Hargraves PE (1988) The Chaetoceros Ehrenberg (Bacillariophyceae) flora of Narragansett Bay, Rhode Island, U.S.A. *Bibliotheca Phycologica* 79: 1–196.
- Rodríguez-Ramírez A, Caballero M, Roy P et al. (2015) Climatic variability and human impact during the last 2000 years in western Mesoamerica: Evidence of late Classic (AD 600–900) and Little Ice Age drought events. *Climate of the Past* 11(9): 1239–1248.
- Romero-Centeno R, Zavala-Hidalgo J and Raga GB (2007) Mid-summer gap winds and low-level circulation over the eastern tropical Pacific. *Journal of Climate* 20(15): 3768–3784.
- Romero OE, Thunell RC, Astor Y et al. (2009a) Seasonal and interannual dynamics in diatom production in the Cariaco Basin, Venezuela. *Deep-Sea Research Part I: Oceanographic Research Papers* 56(4): 571–581.
- Romero OE, Rixen T and Herunadi B (2009b) Effects of hydrographic and climatic forcing on diatom production and export in the tropical southeastern Indian Ocean. *Marine Ecology Progress Series* 384: 69–82.
- Romero OE, Hebbeln D and Wefer G (2001) Temporal and spatial variability in export production in the SE Pacific Ocean: Evidence from siliceous plankton fluxes and surface sediment assemblages. *Deep-Sea Research Part I: Oceanographic Research Papers* 48(12): 2673–2697.
- Romero OE, Leduc G, Vidal L et al. (2011) Millennial variability and long-term changes of the diatom production in the eastern equatorial Pacific during the last glacial cycle. *Paleoceanography* 26(2): 1–11.
- Round FE, Crawford RM and Mann DG (1990) *The Diatoms: Biology & Morphology of the Genera*. Cambridge: The University Cambridge Press.
- Ruiz-Fernández AC, Hillaire-Marcel C, de Vernal A et al. (2009) Changes of coastal sedimentation in the Gulf of Tehuantepec, South Pacific Mexico, over the last 100 years from short-lived radionuclide measurements. *Estuarine, Coastal and Shelf Science* 82(3): 525–536.
- Ruiz-Fernández AC, Maanan M, Sanchez-Cabeza JA et al. (2014) Cronología de la sedimentación reciente y caracterización geoquímica de los sedimentos de la laguna de Alvarado, Veracruz (suroeste del golfo de México). *Ciencias Marinas* 40(4): 291–303.
- Ruiz-Fernández AC, Páez-Osuna F, Machain-Castillo ML et al. (2004) 210Pb geochronology and trace metal fluxes (Cd, Cu and Pb) in the Gulf of Tehuantepec, South Pacific of Mexico. *Journal of Environmental Radioactivity* 76(1-2): 161–175.
- Sachs JP, Sachse D, Smittenberg RH et al. (2009) Southward movement of the Pacific intertropical convergence zone AD 1400–1850. *Nature Geoscience* 2: 519–525.
- Salvatteci R, Gutiérrez D, Field D et al. (2014) The response of the Peruvian upwelling ecosystem to centennial-scale global change during the last two millennia. *Climate of the Past* 10(2): 715–731.
- Sancetta C (1992) Comparison of phytoplankton in sediment trap time series and surface sediments along a productivity gradient. *Paleoceanography* 7(2): 183–194.
- Sancetta C (1995) Diatoms in the Gulf of California: Seasonal flux patterns and the sediment record for the last 15,000 years. *Paleoceanography* 10(1): 67–84.
- Sanchez-Cabeza JA, Rico-Esenaro SD, Corcho-Alvarado JA et al. (2021) Plutonium in coral archives: A good primary marker for an anthropocene type section. *The Science of the Total Environment* 771: 145077.
- Sanchez-Cabeza JA and Ruiz-Fernández AC (2012) 210Pb sediment radiochronology: An integrated formulation and classification of dating models. *Geochimica et Cosmochimica Acta* 82: 183–200.
- Sanchez-Cabeza JA, Ruiz-Fernández AC, Ontiveros-Cuadras JF et al. (2014) Monte Carlo uncertainty calculation of 210Pb chronologies and accumulation rates of sediments and peat bogs. *Quaternary Geochronology* 23: 80–93.
- Sautter LR and Sancetta C (1992) Seasonal associations of phytoplankton and planktic foraminifera in an upwelling region and their contribution to the seafloor. *Marine Micropaleontology* 18(4): 263–278.
- Schrader H, Swanberg N, Lycke AK et al. (1993) Diatom-inferred productivity changes in the eastern equatorial Pacific: The quaternary record of ODP leg 111, site 677. *Hydrobiologia* 269-270: 137–151.
- Schrader HJ and Gersonde R (1978) Diatoms and silicoflagellates. In: Zachariasse WJ (ed) *Microplaeontological counting methods and techniques - an exercise on an eight metres section of the lower Pliocene of Capo Rossello, Sicily*. Odijk: Utrecht Micropaleontology Bulletin, 129–176.
- Sifeddine A, Gutiérrez D, Ortlieb L et al. (2008) Laminated sediments from the central Peruvian continental slope: A 500 year record of upwelling system productivity, terrestrial runoff and redox conditions. *Progress in Oceanography* 79(2-4): 190–197.
- Smrzka D, Zwicker J, Bach W et al. (2019) The behavior of trace elements in seawater, sedimentary pore water, and their incorporation into carbonate minerals: A review. *Facies* 65(4): 1–47.
- Staines-Urías F, Douglas RG and Gorsline DS (2009) Oceanographic variability in the southern Gulf of California over the past 400 years: Evidence from faunal and isotopic records from planktic foraminifera. *Palaeogeography Palaeoclimatology Palaeoecology* 284(3-4): 337–354.
- Thunell RC and Kepple AB (2004) Glacial-Holocene  $\delta^{15}N$  record from the gulf of Tehuantepec, Mexico: Implications for denitrification in the eastern equatorial Pacific and changes in atmospheric N<sub>2</sub>O. *Global Biogeochemical Cycles* 18(1): 1–12.
- Torres-Ariño A, Okolodkov YB and Herrera-herrera NV (2019) Un listado del fitoplancton y microfítobentos del sureste del pacífico mexicano A checklist of phytoplankton and

- microphytobenthos of the southeastern Mexican Pacific. *Cymbella* 5(1): 1–97.
- Trasviña A, Barton ED, Brown J et al. (1995) Offshore wind forcing in the Gulf of Tehuantepec, Mexico: The asymmetric circulation. *Journal of Geophysical Research* 100(C10): 20649–20663.
- Treinen-Crespo C, Barbara L, Villaescusa JA et al. (2021) Revisiting the marine reservoir age in Baja California continental margin sediments using  $^{14}\text{C}$  and  $^{210}\text{Pb}$  dating. *Quaternary Geochronology* 66: 101178.
- Treppke UF, Lange CB and Wefer G (1996) Vertical fluxes of diatoms and silicoflagellates in the eastern equatorial Atlantic, and their contribution to the sedimentary record. *Marine Micropaleontology* 28: 73–96.
- Tribovillard N, Algeo TJ, Lyons T et al. (2006) Trace metals as paleoredox and paleoproductivity proxies: An update. *Chemical Geology* 232(1–2): 12–32.
- Vázquez-Selem L (2011) Las glaciaciones en las montañas del centro de México. In: Caballero M and Ortega B (eds) *Escenarios de Cambio Climático: Registros Del Cuaternario En América Latina I*. México: Universidad Nacional Autónoma de México, pp.215–238.
- Yamaguchi R and Suga T (2019) Trend and variability in global Upper-Ocean stratification since the 1960s. *Journal of Geophysical Research Oceans* 124(12): 8933–8948.
- Yan H, Sun L, Wang Y et al. (2011) A record of the Southern Oscillation index for the past 2,000 years from precipitation proxies. *Nature Geoscience* 4(9): 611–614.